RESEARCH ARTICLE • OPEN ACCESS

A Non-linear Fractional Model for Analyzing the Impact of Vaccination on the Dynamics of COVID-19 in Indonesia

John Olajide Akanni *et al.*

Volume 6, Issue 2, Pages 109–128, June 2025

Received 30 January 2025, Revised 3 April 2025, Accepted 8 June 2025, Published Online 24 June 2025

To Cite this Article : J. O. Akanni *et al.*,"A Non-linear Fractional Model for Analyzing the Impact of Vaccination on the Dynamics of COVID-19 in Indonesia", *Jambura J. Biomath*, vol. 6, no. 2, pp. 109–128, 2025, *https://doi.org/10.37905/jjbm.v6i2.30383*

© 2025 by author(s)

JOURNAL INFO • JAMBURA JOURNAL OF BIOMATHEMATICS

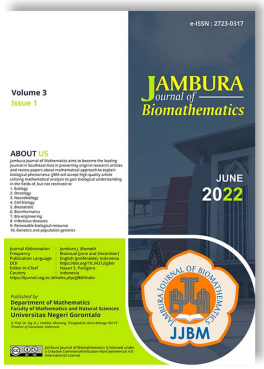

Homepage	:	http://ejurnal.ung.ac.id/index.php/JJBM/index
Journal Abbreviation	:	Jambura J. Biomath.
Frequency	:	Quarterly (March, June, September and December)
Publication Language	:	English
DOI	:	https://doi.org/10.37905/jjbm
Online ISSN	:	2723-0317
Editor-in-Chief	:	Hasan S. Panigoro
Publisher	:	Department of Mathematics, Universitas Negeri Gorontalo
Country	:	Indonesia
OAI Address	:	http://ejurnal.ung.ac.id/index.php/jjbm/oai
Google Scholar ID	:	XzYgeKQAAAAJ
Email	:	editorial.jjbm@ung.ac.id

JAMBURA JOURNAL • FIND OUR OTHER JOURNALS

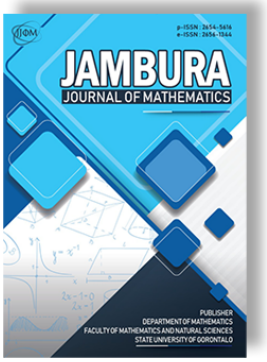

Jambura Journal of Mathematics

Jambura Journal of Mathematics Education

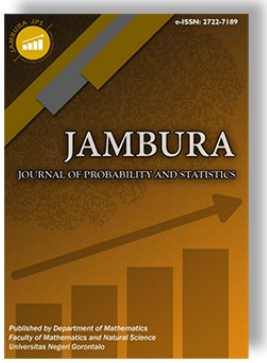

Jambura Journal of Probability and Statistics

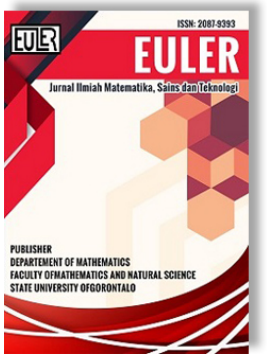

EULER : Jurnal Ilmiah Matematika, Sains, dan Teknologi

Jambura Journal of Biomathematics, Volume 6, Issue 2, Pages 109–128, June 2025 https://doi.org/10.37905/jjbm.v6i2.30383

Research Article

Check for updates

A Non-linear Fractional Model for Analyzing the Impact of Vaccination on the Dynamics of COVID-19 in Indonesia

John Olajide Akanni[1,2], **Afeez Abidemi**[3], **Fatmawati Fatmawati**[4,*], **and Chidozie Williams Chukwu**[5]

[1]*Department of Mathematics, Saveetha School of Engineering SIMATS, Chennai, India*
[2]*Department of Mathematical and Computing Sciences, Koladaisi University, Ibadan, Oyo State, Nigeria*
[3]*Department of Mathematical Sciences, Federal University of Technology Akure, Ondo State, Nigeria*
[4]*Department of Mathematics, Faculty of Science and Technology, Universitas Airlangga, Surabaya 60115, Indonesia*
[5]*Department of Mathematical Sciences, Georgia Southern University, Statesboro Georgia, USA.*

ARTICLE HISTORY
Received 30 January 2025
Revised 3 April 2025
Accepted 8 June 2025
Published 24 June 2025

KEYWORDS
Dynamical system
COVID-19 virus
Bifurcation analysis
Sensitivity analysis
Vaccination

ABSTRACT. *COVID-19, caused by the novel coronavirus SARS-CoV-2, remains a global public health challenge. This study proposes and analyzes a mathematical model to monitor the progression of COVID-19 and assess the impact of immunization efforts. The model incorporates key epidemiological factors and is calibrated using publicly available data on cumulative daily cases of COVID-19 in Indonesia, spanning from July 1, 2021, to July 21, 2022. The basic reproduction number, $\mathcal{R}_0$, is derived and the equilibrium states are established. Bifurcation analysis is conducted using the Center Manifold Theorem to understand the potential transition dynamics of the disease. A local sensitivity analysis reveals that the effective transmission rate (β), the natural mortality rate (μ), the vaccination rate (τ) and the treatment rate for symptomatic individuals (θ) are the most influential parameters. Model simulations suggest that reducing transmission, improving treatment, and increasing vaccine uptake significantly reduce disease burden. To better capture the memory effect inherent in disease transmission, the model is extended to a fractional-order Caputo derivative framework. The existence, uniqueness, and stability of the fractional model are established via fixed-point theory. Numerical results demonstrate that the decrease in fractional order slightly shifts the dynamics, suggesting behavioural changes in response to past outbreaks. These findings provide valuable information on disease control strategies and highlight the importance of sustained public health measures.*

This article is an open access article distributed under the terms and conditions of the Creative Commons Attribution-NonComercial 4.0 International License. Editorial of JJBM: Department of Mathematics, Universitas Negeri Gorontalo, Jln. Prof. Dr. Ing. B. J. Habibie, Bone Bolango 96554, Indonesia.

1. Introduction

Severe acute respiratory syndrome coronavirus 2 (SARS-CoV-2) was responsible for the first outbreak of COVID-19 in Wuhan, Hubei province, China in December 2019 [1–4]. Numerous SARS-CoV-2 variants have been discovered as a result of the high mutation rate and severity of the virus [5, 6]. However, the rate at which the virus is distributed has been extremely high as it can be transmitted from one person to another [7, 8]. This has been a serious concern and a worldwide burden, eventually led the World Health Organization (WHO) to eventually announce the virus as a global pandemic. Having been widely spread worldwide, it has become a subject of concern for public health practitioners. The governments of nations have also taken serious precautions, as it causes economic instability [3, 4, 9]. To this end, people in different societies suffered the negative impact of pestilence [10]. WHO released statistics totaling approximately 248,467,363 confirmed cases, of which 5,027,183 persons died, while 7,027,377,238 vaccine doses were administered worldwide as of November 4, 2021 [2, 10].

Mathematical modelling plays an important role in exploring the dissemination modalities of diseases and how government agents can efficiently set goals to fight against disease outbreaks. Bernoulli [11] constructed a mathematical model that serves as an important tool to understand the modalities of infectious diseases. Similarly, Kermack and McKendrick [12] proposed mathematical models to give a framework that can be used to understand the modalities of infectious diseases. Numerous scholars have explored the dispatching modalities of viruses and varied models in their findings by studying and extending the susceptible, exposed, infected, removed (SEIR) mathematical model with a significant cavity that can track and communicate real-life issues. Kemp *et al.* [13] studied different types of viral infection and hospitalization, the updated SEIR model, and included interactions between vaccination and social factors. This model consider social interaction criteria to determine the vaccination coverage required to achieve herd immunity in 2021. Treesatayapun [14] applied the SEIR model to account for the quarantined population and the effect of the vaccination rate, and it was concluded that the application of vaccination at the optimal rate is the best intervention. Rafiq *et al.* [15] introduced a new coding system that produces realistically oriented results from complex bimodal nonlinear models. Acheampong *et al.* [16] defined the dispatch

*Corresponding Author.

Email : *fatmawati@fst.unair.ac.id* (F. Fatmawati)
Homepage : http://ejurnal.ung.ac.id/index.php/JJBM/index / E-ISSN : 2723-0317
© 2025 by the Author(s).

modalities in Ghanaian with severe acute respiratory failure evaluating the fundamental threshold number, a modified compartmental model $SEIR$ was built. Liu *et al.* [17] have put forward an epidemiological model which is $SEIR$ in nature applying a Bayesian principle that sheds more light on the dispatching procedures in England's nine regions. In Kassa *et al.* [18] the alleviation techniques for COVID-19 and a sensitivity illustration were critically examined. These two authors, Sharov [19] and Tong *et al.* [20], attempted to determine the shutdown of the potency to regulate the transmission of viral diseases and recommended that such a model can be modified. Pai *et al.* [21] reviewed confinement and its consequences, which are used in India to stop the spread of COVID-19, and assessed infection-transmitting procedures. Huang *et al.* [22] abandoned the disease model that showed staying indoors was a poorer approach than a coordinated effort of immunization and keeping some distance. Sahin [23] compiled the relationship between three different models that specify the accuracy of the total COVID-19 instances that have been verified to date.

In other similar studies, Kuddus *et al.* [24] scrutinized the outcome of two doses of vaccination, progression, and dispatch rate in the sweep of measles and found that the dispatch rate (β) from susceptible to exposed individuals had the most substantial consequence on the prevalence of measles. Sen *et al.* [25] investigated the impact of double-dose immunization, a new epidemic $SEIR$ was expressed. In the same line of argument, Gomes *et al.* [26] posited that vaccines assist in acquiring of herd immunity among individuals. Moore *et al.* [27] developed a non-linear mathematical model to determine the vaccine efficacy in managing the protracted coronavirus patterns, and the model analysis showed that merely double dose vaccination is inadequate to stop the epidemic. They also said that vaccination would stave off an estimate of 85% of the infection. Yang *et al.* [28] surveyed the impact of alleviation and suppression, which also includes a number of continuous measures that will curb the spread of COVID-19 in the UK and other parts of Europe. The authors concluded that to equalize the demand for healthcare, a rolling intervention is necessary, which was suggested to be one of the best strategies to curtail general maladies and casualties as a result of the virus, which also efficiently balances the health needs of the UK [28]. Sah *et al.* [23] asserted that the burden caused by multiple variations of coronaviruses can be reduced by accelerating vaccine deployment. Martnez-Rodrguez *et al.*, [29] considered various burden scenarios caused by the SARS-CoV-2 virus and also examined the impact of vaccination speed and effectiveness on coronavirus prevalence, hospitalizations, and casualties.

Fuady *et al.* [30] demonstrated and started various methods to make the vaccine available. Ramos *et al.* [31] also developed a mathematical model to assess how variations in coronaviruses and vaccines will affect the situation. Arruda *et al.* [32] developed an epidemic model that evaluated virus replication and a variety of viral tendencies, which are the latest threat to the prevention of COVID-19. Leónet *et al.* [33] explained the various inclinations of COVID-19 and developed a brand-new disease model that supports two distinct viral variants and the implications of vaccination-focused programs. In low and middle-income countries (third world), COVID-19 vaccination is highly cost effective [24]. Before the beginning of medication and vaccination control measures, other management criteria such as self-isolation, masking of the face, washing hands, social or physical distancing, complete lockdowns, and closing or restricted openings of stores and schools have been established [34–40]. In [41], the author suggested and studied a mathematical model of COVID-19, considering the available therapeutic measures, vaccinating the vulnerable, and providing medical service to those who have contracted the disease. The suggested model includes certain epidemiological and biological elements of COVID-19, including demographic parameters, optimal supervision, and description of sensitivity. To our knowledge, the study without saying provides the primary in-depth mathematical example of the qualitative modalities of COVID-19 with inadequate vaccine and medication.

Recent studies have advanced the application of fractional-order differential equations in epidemiological modeling. Yaseen et al. [42] developed a fractional-order cholera model incorporating asymptomatic carriers and a Holling type-II functional response, establishing global asymptotic stability and conducting sensitivity analysis. In a similar vein, Yaseen et al. [43] enhanced hepatitis B and C transmission models by integrating vaccination strategies, proving global stability and highlighting the impact of fractional derivatives on model dynamics. Mohsen et al. [44] proposed a COVID-19 model incorporating curfew strategies, demonstrating the model's global stability and the effectiveness of quarantine measures in controlling the pandemic. Additionally, Ali and Naji [45] conducted a dynamical analysis within-host and between-host for HIV/AIDS, applying optimal control strategies to model disease spread. Their study incorporated various interventions such as vaccination, therapeutic dosing, and public health campaigns, demonstrating the effectiveness of these strategies in controlling HIV/AIDS dynamics. These studies underscore the utility of fractional-order models in capturing complex dynamics and informing public health strategies.

In this study, we propose a comprehensive mathematical model that integrates vaccination, treatment, and public behavioural responses to monitor and predict the transmission dynamics of COVID-19 in Indonesia. The model is calibrated with real-world data from July 1, 2021, to July 21, 2022. We apply the next-generation matrix method to compute the basic reproduction number, investigate the disease-free and endemic equilibrium states, and perform a sensitivity analysis to identify the most impactful epidemiological parameters. One of the significant contributions of this study is the extension of the integer-order model to a fractional-order Caputo model to capture memory effects in disease transmission. We establish the existence, uniqueness, and stability of the fractional model using fixed-point theory, and we analyze how fractional-order dynamics influence the model's behaviour and the susceptible population. Our findings emphasize the importance of sustained public health interventions, such as reducing the transmission rate β, enhancing treatment capacity, and increasing vaccine uptake, in minimizing the burden of COVID-19. The insights from this model provide health authorities with a valuable decision-making framework to strengthen control efforts in Indonesia and similar epidemiological settings.

The rest of this research is sectioned as follows: Section 2 discusses the mathematical formulation of the COVID-19 model

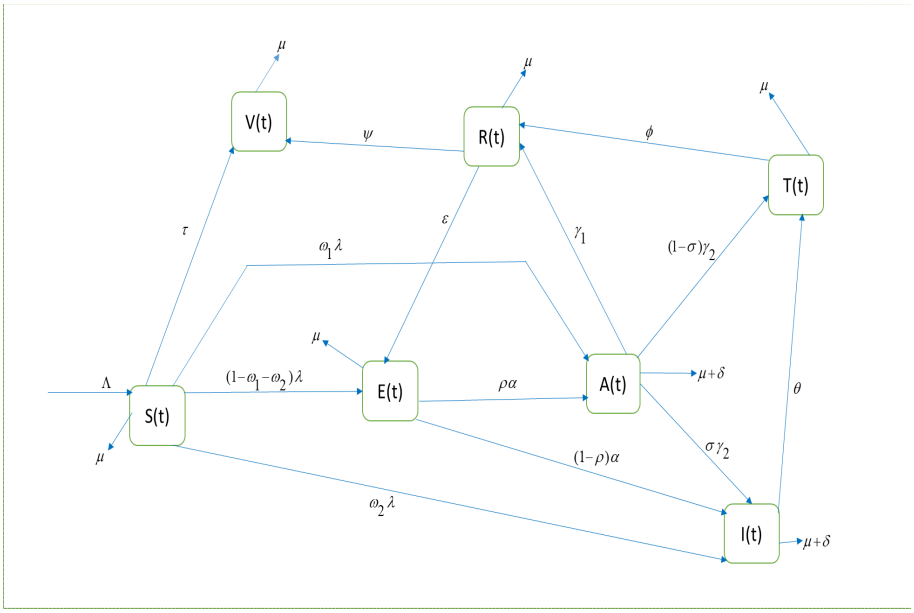

Figure 1. Flowchart for the model (2)

and its basic qualitative properties, while the existence of the model's equilibrium points, and their stability analysis are considered in Section 3. The model is further investigated for the bifurcation property in this section. In addition, in Section 4, the fitting of the data and the estimation of parameters are discussed. With appropriate parameter values, the numerical simulations of the proposed model and the sensitivity analysis are explored in Section 6. Finally, Section 7 presents some concluding remarks explaining the results of our modelling framework.

2. Model formation and its basic qualitative properties

2.1. *Model formation*

This section considers the formulation of an epidemic model which concentrates on the impact of vaccination on COVID-19 disease in a population. The total population at any time t denoted as $N(t)$, is sub-divided into seven mutually exclusive compartments, namely, susceptible class, $S(t)$ (those likely to contract COVID-19 infection), exposed class, $E(t)$ (those contaminated but not infectious yet), asymptomatic class, $A(t)$ (those infected with mild symptoms and are capable of the disease spread), infectious class, $I(t)$ (those who exhibits symptoms of COVID-19 and are capable of the disorder spread), treatment class, $T(t)$ (those who are infectious and under treatment due to COVID-19), recovered class, $R(t)$ (those who have recovered from COVID-19 infection) and vaccinated class, $V(t)$ (those who have received the vaccine against COVID-19 disease). Thus,

$$N(t) = S(t) + E(t) + A(t) + I(t) + T(t) + R(t) + V(t). \quad (1)$$

Table 1 defines the parameters used in model (2) and the model's scheme is shown in Figure 1.

$$\begin{aligned}
\frac{dS}{dt} &= \Lambda - \lambda S - (\mu + \tau)S,\\
\frac{dE}{dt} &= (1 - \omega_1 - \omega_2)\lambda S - (\alpha + \mu)E + \varepsilon R,\\
\frac{dA}{dt} &= \omega_1 \lambda S - (\gamma_1 + \gamma_2 + \delta + \mu)A + \rho\alpha E,\\
\frac{dI}{dt} &= \omega_2 \lambda S + (1 - \rho)\alpha E + \sigma\gamma_2 A - (\theta + \delta + \mu)I, \quad (2)\\
\frac{dT}{dt} &= (1 - \sigma)\gamma_2 A + \theta I - (\mu + \phi)T,\\
\frac{dR}{dt} &= \gamma_1 A - (\varepsilon + \mu)R + \psi V + \phi T,\\
\frac{dV}{dt} &= \tau S - (\psi + \mu)V,
\end{aligned}$$

with initial conditions when $t = 0$, and the force of infection is $\lambda = \frac{\beta(I+\eta_1 A+\eta_2 T)}{N}$.

Table 1. Definition of each parameter of model (2)

Parameter	Description
Λ	Recruitment rate
β	Transmission rate
μ	Natural mortality rate
τ	Vaccination rate of susceptible class
δ	Induced death rate of the asymptomatic and infected class
$1 - \omega_1 - \omega_2$	Fraction of susceptible class that moves to the exposed class
ϕ	Treatment rate of the infected class
θ	Progression rate of infected to treatment class
ψ	Fraction of vaccination class that moves to recovered class
α	Progression rate of exposed class to asymptomatic and infected class
γ_1	Recovery rate of the asymptomatic class due to natural immunity
γ_2	Progression rate of asymptomatic class to infected and treatment class
ε	Rate at which recovered class moves back to the exposed class
η_1, η_2	Modification parameter for the asymptomatic and exposed class, respectively.
ω_1, ω_2	Fractions of the susceptible that moves to asymptomatic and exposed classes, respectively.
$\sigma, 1 - \sigma$	Fraction of the of asymptomatic class that moves to infected and treatment class, respectively.
$\rho, 1 - \rho$	Fractions of the exposed class that progress to asymptomatic and infected class respectively

2.2. Fundamental qualitative properties of model (2)

The fundamental qualitative trait of the model (2), concerning the positive boundedness of solutions, will now be explored. Given that all parameters are non-negative, it is imperative to demonstrate the state variables' non-negativity for all times.

Theorem 1. *For all times $t > 0$, solutions of said model (2) having non-negative initial values $S(0)$, $E(0)$, $A(0)$, $I(0)$, $T(0)$, $R(0)$, $V(0)$ remain non-negative.*

Proof. We can be rewrite the S class of system (2) as

$$\frac{dS}{dt} + \lambda S(t) + (\mu + \tau)S(t) \geq 0. \tag{3}$$

Integrating eq. (3), gives

$$\frac{d}{dt}\left[S(t)\exp\left\{(\mu+\tau)t + \int_0^t \lambda(\varpi)d\varpi\right\}\right] \geq 0. \tag{4}$$

eq. (4) leads to

$$S(t) \geq S(0)\exp\left\{-\left[(\mu+\tau)t + \int_0^t \lambda(\varpi)d\varpi\right]\right\} > 0,$$

for all values of t greater than 0. The same methodology may be used to demonstrate that the remaining state variables $E(t)$,A(t), $I(t)$,T(t), $R(t)$, and $V(t)$ are non-negative for all time $t > 0$. □

Moreover, it is important to mention that the COVID-19 model (2) is shown to be biologically feasible in region

$$\Gamma = \left\{(S(t), E(t), A(t), I(t), T(t), R(t), V(t)) \in \mathbb{R}_+^7 : N \leq \frac{\Lambda}{\mu}\right\},$$

and by proven technique from the literature [46–48], the region Γ can easily be proved to be positively invariant. Thus, there are all solutions in the region Γ where the COVID-19 model (2) is mathematically sound and well-posed in terms of epidemiology [49].

3. Existence of equilibrium and stability analysis

This section establishes the existence of steady-state solutions (equilibrium points) for the model (2) and examines the type of bifurcation it exhibits.

3.1. Disease-free equilibrium

The model (2) disease-free equilibrium, denoted by $\mathcal{D}_0$, is provided by

$$\begin{aligned}\mathcal{D}_0 &= (S_0, E_0, A_0, I_0, T_0, R_0, V_0),\\ &= \left(\frac{\Lambda}{\mu+\tau}, 0, 0, 0, 0, 0, \frac{\tau\Lambda}{(\psi+\mu)(\mu+\tau)}\right).\end{aligned} \tag{5}$$

The local stability of $\mathcal{D}_0$ is proved using the method and the approach in [50]. It can be seen from model (2) that

$$\begin{aligned}\frac{d}{dt}\begin{pmatrix}E\\A\\I\\T\end{pmatrix} &= \begin{pmatrix}(1-\omega_1-\omega_2)\frac{\beta(I+\eta_1 A+\eta_2 T)}{N}S\\ \omega_1\frac{\beta(I+\eta_1 A+\eta_2 T)}{N}S\\ \omega_2\frac{\beta(I+\eta_1 A+\eta_2 T)}{N}S\\ 0\end{pmatrix}\\ &\quad - \begin{pmatrix}(\alpha+\mu)E - \varepsilon R\\ (\gamma_1+\gamma_2+\delta+\mu)A - \rho\alpha E\\ -(1-\rho)\alpha E - \sigma\gamma_2 A + (\theta+\delta+\mu)I\\ -(1-\sigma)\gamma_2 - \theta I + (\phi+\mu)T\end{pmatrix}.\end{aligned} \tag{6}$$

Now, using the next generation matrix method study in depth by [50], widely used in the literature (for example, see [38, 48, 51, 52]), it follows from eq. (6) that the matrix F of new infection terms and matrix V of the transition terms are given, respectively, as

$$F = \begin{pmatrix}0 & \frac{(1-\omega_1-\omega_2)\beta\eta_1}{(\mu+\tau)} & \frac{(1-\omega_1-\omega_2)\beta\mu}{(\mu+\tau)} & \frac{(1-\omega_1-\omega_2)\beta\eta_2\mu}{(\mu+\tau)}\\ 0 & \frac{\omega_1\beta\eta_1\mu}{(\mu+\tau)} & \frac{\omega_1\beta\mu}{(\mu+\tau)} & \frac{\omega_1\beta\eta_2\mu}{(\mu+\tau)}\\ 0 & \frac{\omega_2\beta\eta_1\mu}{\mu+\tau} & \frac{\omega_2\beta\mu}{(\mu+\tau)} & \frac{\omega_2\beta\eta_2\mu}{(\mu+\tau)}\\ 0 & 0 & 0 & 0\end{pmatrix},$$

$$V = \begin{pmatrix}(\alpha+\mu) & 0 & 0 & 0\\ -\rho\alpha & (\gamma_1+\gamma_2+\delta+\mu) & 0 & 0\\ (1-\rho)\alpha & -\sigma\gamma_2 & (\theta+\delta+\mu) & 0\\ 0 & -(1-\sigma)\gamma_2 & -\theta & (\mu+\phi)\end{pmatrix}. \tag{7}$$

As a result, the effective (or control) reproduction number of the model (2) is calculated using the formula $\mathcal{R}_0 = \rho(FV^{-1})$, where ρ is the radius of the spectra of FV^{-1}. Thus,

$$\begin{aligned}\mathcal{R}_0 &= \frac{\beta\mu(d_5a_1 + a_2d_5 + a_3d_4d_5 + \eta_2n_1)}{d_1d_2d_3d_4d_5},\\ a_1 &= \alpha(1-\omega_1-\omega_2)(\sigma\rho\gamma_2 + d_3(1-\rho)),\\ a_2 &= d_2(\sigma\omega_1\gamma_2 + d_3\omega_2),\\ a_3 &= \eta_1(\alpha\rho(1-\omega_1-\omega_2) + d_2\omega_1),\\ d_1 &= \mu+\tau,\\ d_2 &= \mu+\alpha,\\ d_3 &= \gamma_1+\gamma_2+\delta+\mu,\\ d_4 &= \theta+\delta+\mu,\\ d_5 &= \mu+\phi,\\ d_6 &= \mu+\varepsilon,\\ d_7 &= \mu+\psi,\\ n_1 &= \gamma_2(\alpha\rho(1-\omega_1-\omega_2) + d_2\omega_1)(\sigma\theta + d_4(1-\sigma))\\ &\quad + d_3\theta(\alpha(1-\rho)(1-\omega_1-\omega_2) + d_2\omega_2),\end{aligned} \tag{8}$$

which can be expressed further as

$$\begin{aligned}\mathcal{R}_0 &= \frac{\beta\mu(a_1+a_2)}{d_1d_2d_3d_4} + \frac{\beta\mu a_3}{d_1d_2d_3} + \frac{n_1\beta\mu\eta_2}{d_1d_2d_3d_4d_5},\\ &= \mathcal{R}_{0I} + \mathcal{R}_{0A} + \mathcal{R}_{0T}.\end{aligned} \tag{9}$$

The tested technique establishes the following outcome (see Theorem 2 of [50]). The spread potential of COVID-19 in a population with the presence of vaccination governed by the model (2)

is quantified by the threshold number $\mathcal{R}_0$. When the control reproduction number $\mathcal{R}_0$ is greater than unity, the disease persists in the population, but when it is less than unity, the disease dies out in the population.

Lemma 1. *The $\mathcal{D}_0$, which is the disease-free equilibrium of the model, is locally asymptotically stable in Γ if $\mathcal{R}_0 < 1$ and unstable if $\mathcal{R}_0 > 1$.*

The spread potential of the COVID-19 population in a population under the control of a model (2) is shown by the fundamental threshold number $\mathcal{R}_0$. If the initial sizes of the model subpopulations are in the region of affinity for disease-free equilibrium, then the epidemiological meaning of Lemma 1 is that the spread of COVID-19 can be kept in check in the population when $\mathcal{R}_0 < 1$.

3.2. Existence of endemic equilibrium $\mathcal{E}^{**}$

The steady-state solution of the model (2) when all state variables are non-zero and positive is referred to as the endemic equilibrium point (EEP) denoted and given by

$$\mathcal{E}^{**} = (S^{**}, E^{**}, A^{**}, I^{**}, T^{**}, R^{**}, V^{**}). \tag{10}$$

Now, let us define the force of infection at the endemic state by

$$\lambda^{**} = \frac{\beta(I^{**} + \eta_1 A^{**} + \eta_2 T^{**})}{N^{**}}. \tag{11}$$

So, a special endemic equilibrium point is found when the following condition is met $\omega_1 = \omega_2 = \delta = 0$. Then, setting the right-hand sides of the model (2) to zero when this condition has been imposed, the following system is obtained in terms of λ^{**}:

$$\begin{aligned}
S^{**} &= \frac{\Pi}{\lambda^{**} + d_1},\\
E^{**} &= \frac{\Lambda\lambda^{**} d_3 d_4 d_5 d_6 \rho\alpha}{\rho\alpha(\lambda^{**} + d_1)(d_2 d_3 d_4 d_5 d_6) - \alpha a_0)},\\
A^{**} &= \frac{\Lambda\lambda^{**} d_4 d_5 d_6 \rho\alpha}{(\lambda^{**} + d_1)(d_2 d_3 d_4 d_5 d_6) - \alpha a_0)},\\
I^{**} &= \frac{((1-\rho)\alpha d_3 + \sigma\gamma_2\rho\alpha)\lambda^{**}\Lambda d_5 d_6}{(d_2 d_3 d_4 d_5 d_6 - \alpha a_0)(\lambda^{**} + d_1)},\\
T^{**} &= \frac{((1-\sigma)\gamma_2 d_4\rho\alpha + \theta((1-\rho)\alpha d_3 + \sigma\gamma_2\rho\alpha)}{(d_2 d_3 d_4 d_5 d_6 - \alpha a_0)(\lambda^{**} + d_1)},\\
R^{**} &= \frac{\gamma_1 d_4 d_5 \rho\alpha + \phi((1-\sigma)\gamma_2 d_4\rho\alpha + \theta((1-\rho)\alpha d_3 + \theta\gamma_2\rho\alpha))}{d_2 d_3 d_4 d_5 d_6 d_7(d_4 d_5 d_6\rho\alpha},\\
V^{**} &= \frac{\tau\Lambda}{d_1 d_7(\lambda^{**} + d_1)},
\end{aligned} \tag{12}$$

where

$$a_0 = \gamma_1 d_4 d_5 \rho\alpha + \phi((1-\sigma)\gamma_2 d_4\rho\alpha + \theta((1-\rho)\alpha d_3 + \sigma\gamma_2\rho\alpha),$$

and

$$N^{**} = S^{**} + E^{**} + A^{**} + I^{**} + T^{**} + R^{**} + V^{**}. \tag{13}$$

Substituting eqs. (12) and (13) into equation eq. (11) and after algebraic manipulations, gives the following

$$\lambda^{**} = 0 \text{ or } X_1\lambda^{**} + X_2 = 0. \tag{14}$$

When $\lambda^{**} = 0$ in the model (12), it means that EEP ($\mathcal{E}^{**}$) does not exist, but there exists EEP when $X_1\lambda^{**} + X_2 = 0$. Also, a unique $\mathcal{E}^{**}$ exist when $\mathcal{R}_0 > 1$, where

$$X_1 = d_2 d_3 d_4 d_5 d_6\alpha \text{ and } X_2 = d_2 d_3 d_4 d_5 d_6\alpha(1 - \mathcal{R}_0).$$

If $\mathcal{R}_0 > 1$, then there exists a unique endemic equilibrium.

Lemma 2. *The model (2) has a unique endemic equilibrium ($\mathcal{E}^{**}$), whenever $\mathcal{R}_0 > 1$.*

4. Model fitting and parameter estimation

To validate our model and estimate the parameter values, we fit model (2) to cumulative daily reported new cases of COVID-19, as discussed in this section. We used the daily COVID-19 incidence data from July 1, 2021 to July 21, 2022, for Indonesia publicly available on [53] to parameterize our model after achieving the best fit to help obtain the unknown model parameters. The demographic data Λ and μ are estimated from [53]. We assume the value of the modification parameter for the treatment class (η_2) relative to the infectiousness of treated individuals compared to those of infected asymptomatic and symptomatic individuals, the values for parameters α, γ_1, ψ, ϕ and η_1 are taken from established literature, while the set of parameters $\Psi = (\beta, \tau, \omega_1, \omega_2\varepsilon, \gamma_2, \delta, \rho, \sigma, \theta)$ is fitted to the accurate COVID-19 data reported for Indonesia. To train the COVID-19 model (2) with the cumulative daily reported cases of COVID-19, $C(t)$ is considered the cumulative number of reported (detected) cases so that the rate of change of $C(t)$ with respect to time is proportional to infected persons asymptomatic and symptomatic according to the model's prediction eq. (2). Thus, $C(t)$ can be obtained as the solution of the differential equation given by

$$\frac{dC(t)}{dt} = (1-\sigma)\gamma_2 A(t) + \theta I(t). \tag{15}$$

In the sense of [34, 51, 54, 55], the fitting process is executed with `fmincon` software package in MATLAB using the least squares method with a view to optimizing the summation of squared errors

$$J(\Psi) = \sum (C(t, \Psi) - C_{real})^2,$$

subject to the COVID-19 model (2), where $C(t, \Psi)$ is the solution of the model related to the number of daily reported cases of COVID-19 over time t, Ψ is the target set of estimated parameters, while C_{real} is real data of COVID-19 daily reported cases. The Indonesian population was estimated at $273,753,191$ in 2021 [53]. Then we fix the total population at time $t = 0$ at $N(0) = 273753191$. In 2021, the average lifespan of Indonesians was 71.72 years. Thus, the demographic parameter μ is estimated as $\mu = 1/(71.72 \times 365)$ per day. In the absence of COVID-19 infection, the limiting total population is considered as $\frac{\Lambda}{\mu} = 273753191$, so that $\Lambda = 10457.46$ per day. In addition, we set $\alpha = 1/5.2$ per day, $\phi = 1/15$ per day and $\eta_1 = 0.5$ [55] and assume that $\gamma_1 = 1/15$ per day and $\psi = 1/15$ per day. We further assume that the transmissibility of treated/hospitalized infection is $1/4$ times that of symptomatic infection, so that $\eta_2 = 0.25$. On 1 July 2021, there were $24,836$ newly reported

Table 2. Estimated values for the parameters used for numerical simulation of model (2) normalized per day.

Parameter	Value	Source	Parameter	Value	Source
Λ	10457.46	Estimated from [53]	ω_1	0.3831	Fitted z
α	$1/5.2$	[55]	γ_1	$1/15$	Assumed
ψ	$1/15$	Assumed	ϕ	$1/15$	[55]
η_1	0.5	[55]	η_2	0.25	Assumed
β	0.5232	Fitted	τ	0.1006	Fitted
μ	$1/(71.72 \times 365)$	Estimated from [53]	ω_2	0.0162	Fitted
ε	0.0011	Fitted	γ_2	0.1536	Fitted
δ	7.9586×10^{-6}	Fitted	ρ	4.2765×10^{-5}	Fitted
σ	0.2259	Fitted	θ	1.2409×10^{-4}	Fitted

cases of COVID-19. On that day, $30,184,392$ people had received at least one vaccine dose, so we set the initial conditions for symptomatic infected individuals I and vaccinated individuals V at time $t = 0$ as $I(0) = 24836$ and $V(0) = 30184392$, respectively. To obtain the solution of $C(t)$ in eq. (15), we assume that $C(0) = I(0) = 24836$. At time $t = 0$, we assume that the number of exposed and asymptotically infected individuals is 20 and 10 times the number of symptomatically infected individuals, respectively, so that $E(0) = 20 \times I(0) = 496720$ and $A(0) = 10 \times I(0) = 248360$. We further assume that at time $t = 0$, there were 24836 people under treatment (hospitalization) and recovery of 20808, hence $T(0) = 24836$ and $R(0) = 20808$. Since $N(0) = 273753191$, it is convenient to estimate the initial value for the susceptible population at time $t = 0$ as $S(0) = N(0)-(E(0)+A(0)+I(0)+T(0)+R(0)+V(0)) = 242753239$. Therefore, the model is fitted to the real COVID-19 data along with the estimated initial conditions above to obtain the values of the target parameters fitted Ψ as presented in Table 2. The estimated control reproduction number for the outbreaks given in Table 2 is approximately $\mathcal{R}_0 = 0.7908$. Figure 2 illustrates the comparison of real data for COVID-19 reported cases in Indonesia and the prediction of the model (2) over the time horizon of $[0,\ 385]$ in days. It is observed that the model fitted well with the cumulative number of daily reported cases of COVID-19.

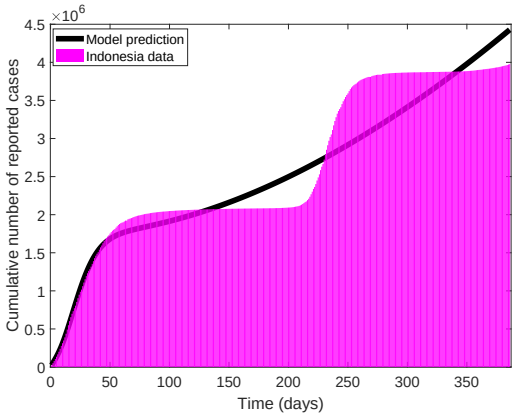

Figure 2. Graphical illustration of the model fitting to the real COVID-19 data from Indonesia between July 1 2021 and July 21 2022

5. Fractional model analysis

This section presents the fractional order of the model. We also present the basic definitions,model formation, and some analysis.

5.1. *Basics definitions of fractional calculus*

This section presents brief essential definitions regarding fractional calculus in Caputo sense.

Definition 1 (see [56].). Consider $y \in \mathcal{C}^m$ be function, then Caputo derivative having fractional order κ in $(m-1,m)$ where $m \in \mathbb{N}$ is defined as:

$$ {}^{C}D_t^{\kappa}(f(t)) = \frac{1}{\Gamma(m-\kappa)} \int_0^t (t-s)^{(m-\kappa-1)} f^{(m)}(s) ds, \tag{16} $$

with $\Gamma(.)$ is the gamma function and ${}^{C}D_t^{\kappa}(f(t))$ tends to $f^{'}(t)$ as $\kappa \longrightarrow 1$.

Definition 2 (see [56]). The corresponding integral with fractional order $\kappa > 0$ of the function f:$\mathbb{R}^+ \longrightarrow \mathbb{R}$ is expressed as follows:

$$ I_t^{\kappa}(f(t)) = \frac{1}{\Gamma(\kappa)} \int_0^t (t-s)^{(\kappa-1)} f(s) ds,\ 0 < \kappa < 1,\ t > 0. \tag{17} $$

Definition 3. Let y^* denote the equilibrium of the Caputo fractional model then:

$$ {}^{C}D_t^{\kappa}(f(t)) = h(t, f(t)),\ \kappa \in (0,1),\ \text{if } h(t, f^*) = 0. \tag{18} $$

5.2. *Fractional model formation*

This section significant on the fractional model formulation of an epidemic model which concentrates on the impact of vaccination on COVID-19 disease in a population which is shown in Figure 1. The susceptible class, $S(t)$ (those likely to contract COVID-19 infection), exposed class, $E(t)$ (those contaminated but not infectious yet), asymptomatic class, $A(t)$ (those infected with mild symptoms and are capable of the disease spread), infectious class, $I(t)$ (those who exhibits symptoms of COVID-19 and are capable of the disorder spread), treatment class, $T(t)$ (those who are infectious and under treatment due to COVID-19), recovered class, $R(t)$ (those who have recovered from COVID-19 infection) and vaccinated class, $V(t)$ (those who have received the vaccine against COVID-19 disease). The total population at

any time t denoted as $N(t)$, comprising of seven mutually exclusive compartments, named above. The definitions of the parameters used in model (2) are given in Table 1 and κ denotes the memory effect, which is mathematically defined as $0 < \kappa \leq 1$. Thus,

$$N(t) = S(t) + E(t) + A(t) + I(t) + T(t) + R(t) + V(t). \quad (19)$$

The fractional derivative model for the COVID-19 in the presence of vaccination in the sense of Caputo is given as

$$\begin{aligned}
{}^{C}D_t^{\kappa} S(t) &= \Lambda^{\kappa} - \frac{\beta^{\kappa} S(I + \eta_1^{\kappa} A + \eta_2^{\kappa} T)}{N} - (\mu^{\kappa} + \tau^{\kappa})S,\\
{}^{C}D_t^{\kappa} E(t) &= (1 - \omega_1^{\kappa} - \omega_2^{\kappa})\frac{\beta^{\kappa} S(I + \eta_1^{\kappa} A + \eta_2^{\kappa} T)}{N} - (\alpha^{\kappa}\\
&\quad + \mu^{\kappa})E + \varepsilon^{\kappa} R,\\
{}^{C}D_t^{\kappa} A(t) &= \omega_1^{\kappa}\frac{\beta^{\kappa} S(I + \eta_1^{\kappa} A + \eta_2^{\kappa} T)}{N} - (\gamma_1^{\kappa} + \gamma_2^{\kappa} + \delta^{\kappa}\\
&\quad + \mu^{\kappa})A + \rho^{\kappa}\alpha^{\kappa} E,\\
{}^{C}D_t^{\kappa} I(t) &= \omega_2^{\kappa}\frac{\beta^{\kappa} S(I + \eta_1^{\kappa} A + \eta_2^{\kappa} T)}{N} + (1 - \rho^{\kappa})\alpha^{\kappa} E\\
&\quad + \sigma^{\kappa}\gamma_2^{\kappa} A - (\theta^{\kappa} + \delta^{\kappa} + \mu^{\kappa})I,\\
{}^{C}D_t^{\kappa} T(t) &= (1 - \sigma^{\kappa})\gamma_2^{\kappa} A + \theta^{\kappa} I - (\mu^{\kappa} + \phi^{\kappa})T,\\
{}^{C}D_t^{\kappa} R(t) &= \gamma_1^{\kappa} A - (\varepsilon^{\kappa} + \mu^{\kappa})R + \psi^{\kappa} V + \phi^{\kappa} T,\\
{}^{C}D_t^{\kappa} V(t) &= \tau^{\kappa} S - (\psi^{\kappa} + \mu^{\kappa})V,
\end{aligned} \quad (20)$$

where $S(t) > 0$, $E(t) \geq 0$, $A(t) \geq 0$, $I(t) \geq 0$, $T(t) \geq 0$, $R(t) \geq 0, V(t) \geq 0$.

5.3. Basic properties of the model

In this section, we established some properties that allow us to consider the model to be mathematically well-posed. Some of them are non-negativity, uniform boundedness, the existence of solutions, uniqueness, disease-free equilibrium, basic reproduction number, and Hyers-Ulam stability.

5.3. Non-negativity, uniform boundedness

Given that

$$\Omega = \{N(t) : N(t) = (S(t), E(t), A(t), I(t), T(t), R(t), V(t)) \in \mathbb{R}_+^7; N(t) \geq 0\}.$$

Theorem 2. *Let $p(x) \in C[u, v]$ and ${}^{C}D_x^{\kappa} \in C(u, v]$ for $0 < \kappa \leq 1$, then*

$$p(x) = p'(x) + \frac{1}{\gamma(\kappa)}({}^{C}D_x^{\kappa} n)(\epsilon)(x - u)^{\kappa}, \quad (21)$$

where $u \leq \epsilon \leq x$, for all $x \in (u, v]$

Theorem 2 will be used to prove that all positive solutions to the model that we are consider are inside the set Ω using the ideas discussed in [57, 58]

Corollary 1. *Assume that $n(x) \in [u, v]$ and ${}_0^{C}D_x^{\kappa} \in (u, v]$ for $0 < \kappa \leq 1$. If ${}_0^{C}D_x^{\kappa} n(0) \geq 0$, $\forall t \in (0, v)$, then the function n does not increase $\forall x \in (0, v)$.*

Theorem 3. *The $\Omega-$ oriented solution to the Covid-19 model (20) has a positive sign.*

Proof. Applying Theorem 3, we show that the solution to the model (20) is positive, thus;

$$\begin{aligned}
{}^{C}D_t^{\kappa} S(t)|_{S=0} &= \Lambda^{\kappa} > 0,\\
{}^{C}D_t^{\kappa} E(t)|_{E=0} &= (1 - \omega_1^{\kappa} - \omega_2^{\kappa})\frac{\beta^{\kappa} S(I + \eta_1^{\kappa} A + \eta_2^{\kappa} T)}{N}\\
&\quad + \varepsilon^{\kappa} R \geq 0,\\
{}^{C}D_t^{\kappa} A(t)|_{A=0} &= \omega_1^{\kappa}\frac{\beta^{\kappa} S(I + \eta_1^{\kappa} A + \eta_2^{\kappa} T)}{N} + \rho^{\kappa}\alpha^{\kappa} E \geq 0,\\
{}^{C}D_t^{\kappa} I(t)|_{I=0} &= \omega_2^{\kappa}\frac{\beta^{\kappa} S(I + \eta_1^{\kappa} A + \eta_2^{\kappa} T)}{N} + (1 - \rho^{\kappa})\alpha^{\kappa} E\\
&\quad + \sigma^{\kappa}\gamma_2^{\kappa} A \geq 0,\\
{}^{C}D_t^{\kappa} T(t)|_{T=0} &= (1 - \sigma^{\kappa})\gamma_2^{\kappa} A + \theta^{\kappa} I \geq 0,\\
{}^{C}D_t^{\kappa} R(t)|_{R=0} &= \gamma_1^{\kappa} A + \psi^{\kappa} V + \phi^{\kappa} T \geq 0,\\
{}^{C}D_t^{\kappa} V(t)|_{V=0} &= \tau^{\kappa} S \geq 0.
\end{aligned}$$

Hence, referring to Corollary 1, it can be said that all the solutions associated with model (20) are nonnegative and belong to Ω. Now, we show that the model is bounded.

Lemma 3. *The set of solutions $\{S, E, A, I, T, R, V\}$ is bounded and positively invariant in*

$$\Omega^* = \left\{(S, E, A, I, T, R, V) \in \mathbb{R}_+^7 : N(t) \leq \frac{\Lambda^{\kappa}}{\mu^{\kappa}}\right\}. \quad (22)$$

Now, summing the all compartments together, we have the Caputo differential equation for the individual total population as

$${}^{C}D_t^{\kappa} N(t) = \Lambda^{\kappa} - \mu^{\kappa} N - \delta^{\kappa}(A + I) \quad (23)$$

From eq. (23), we have

$$\begin{aligned}
{}^{C}D_t^{\kappa} N(t) &\leq \Lambda^{\kappa} - \mu^{\kappa} N,\\
{}^{C}D_t^{\kappa} N(t) + \mu^{\kappa} N &\leq \Lambda^{\kappa}.
\end{aligned} \quad (24)$$

Apply the Laplace transform method to the inequality eq. (24) with $N(t_0) \geq 0$, we arrive at

$$\begin{aligned}
L[{}^{C}D_t^{\kappa} N(t) + \mu^{\kappa} N(t)] &\leq L[\Lambda^{\kappa}]\\
s^{\kappa}(s) - s^{\kappa-1} N(0) + \mu^{\kappa} N(s) &\leq \frac{\Lambda^{\kappa}}{s},\\
N(s) &\leq \frac{\Lambda^{\kappa}}{s(s^{\kappa} + \mu^{\kappa})} + N(0)\frac{s^{(\kappa-1)}}{s^{\kappa} + \mu^{\kappa}}.
\end{aligned}$$

Taking the Laplace inverse gives

$$N(t) \leq \frac{\Lambda^\kappa}{\mu^\kappa} + \left\{ N(0) - \frac{\Lambda^\kappa}{\mu^\kappa} \right\} E_\kappa(-\mu^\kappa t^t),$$

where $E_\kappa(-\mu^\kappa t^t)$ denotes the Mittag-Leffler function, that is, given any parameter, converge to the same value. Hence, the solution is in Ω^*.

Thus, from $N(t)$ the solutions of the model with starting conditions Ω^* stay in Ω^* for all time $t > 0$, and the function $N(t)$ converges as long as $t \longrightarrow \infty$. Since all solutions in $\mathbb{R}^7_+$ tend to congregate around the positively invariant area Ω^*, we have boundedness and the model is well-posed for study. □

5.3. *Existence and uniqueness of the model solution*

This section examines the presence and essence of the solution for the Caputo operator with the aid of fixed point theory. For this, let $\mathcal{B}(\mathcal{X})$ indicate that a Banach space comprises continuous functions with real values over the interval $\mathcal{X} = [0, a]$ with the norm interpreted by $\|S\| = \sup_{t\in\mathcal{G}}|S(t)|$, $\|E\| = \sup_{t\in\mathcal{G}}|E(t)|$, $\|A\| = \sup_{t\in\mathcal{G}}|A(t)|$, $\|I\| = \sup_{t\in\mathcal{G}}|I(t)|$, $\|T\| = \sup_{t\in\mathcal{G}}|T(t)|$, $\|R\| = \sup_{t\in\mathcal{G}}|R(t)|$, $\|V\| = \sup_{t\in\mathcal{G}}|V(t)|$ and the norm $\|(S, E, A, I, T, R, V)\| = \|S\| + \|E\| + \|A\| + \|I\| + \|T\| + \|R\| + \|V\|$.

Proof. The following was obtained after using the Caputo integral in the model (20)

$$\begin{aligned}
S(t) &= S(0) +^C I^\kappa_{0,t} S(t)\left\{ \Lambda^\kappa - \frac{\beta^\kappa S(I + \eta_1^\kappa A + \eta_2^\kappa T)}{N} - (\mu^\kappa + \tau^\kappa)S \right\},\\
E(t) &= E(0) +^C I^\kappa_{0,t} E(t)\left\{ -(\alpha^\kappa + \mu^\kappa)E + \varepsilon^\kappa R + (1 - \omega_1^\kappa - \omega_2^\kappa)\frac{\beta^\kappa S(I + \eta_1^\kappa A + \eta_2^\kappa T)}{N} \right\},\\
A(t) &= A(0) +^C I^\kappa_{0,t} A(t)\left\{ \omega_1^\kappa \frac{\beta^\kappa S(I + \eta_1^\kappa A + \eta_2^\kappa T)}{N} - (\gamma_1^\kappa + \gamma_2^\kappa + \delta^\kappa + \mu^\kappa)A + \rho^\kappa \alpha^\kappa E \right\},\\
I(t) &= I(0) +^C I^\kappa_{0,t} I(t)\left\{ \omega_2^\kappa \frac{\beta^\kappa S(I + \eta_1^\kappa A + \eta_2^\kappa T)}{N} + (1 - \rho^\kappa)\alpha^\kappa E + \sigma^\kappa \gamma_2^\kappa A - (\theta^\kappa + \delta^\kappa + \mu^\kappa)I \right\},\\
T(t) &= T(0) +^C I^\kappa_{0,t} T(t)\left\{ (1 - \sigma^\kappa)\gamma_2^\kappa A + \theta^\kappa I - (\mu^\kappa + \phi^\kappa)T \right\},\\
R(t) &= R(0) +^C I^\kappa_{0,t} R(t)\left\{ \gamma_1^\kappa A - (\varepsilon^\kappa + \mu^\kappa)R + \psi^\kappa V + \phi^\kappa T \right\},\\
V(t) &= V(0) +^C I^\kappa_{0,t} V(t)\left\{ \tau^\kappa S - (\psi^\kappa + \mu^\kappa)V \right\},
\end{aligned} \tag{25}$$

Arising from Definition 2, the following were obtained,

$$\begin{aligned}
S(t) &= S(0) + \frac{1}{\Gamma(\kappa)}\int_0^t (t-\nu)^{\kappa-1} K_1(\nu, S(\nu))d\nu,\\
E(t) &= E(0) + \frac{1}{\Gamma(\kappa)}\int_0^t (t-\nu)^{\kappa-1} K_2(\nu, E(\nu))d\nu,\\
A(t) &= A(0) + \frac{1}{\Gamma(\kappa)}\int_0^t (t-\nu)^{\kappa-1} K_3(\nu, A(\nu))d\nu,\\
I(t) &= I(0) + \frac{1}{\Gamma(\kappa)}\int_0^t (t-\nu)^{\kappa-1} K_4(\nu, I(\nu))d\nu,\\
T(t) &= T(0) + \frac{1}{\Gamma(\kappa)}\int_0^t (t-\nu)^{\kappa-1} K_5(\nu, T(\nu))d\nu,\\
R(t) &= R(0) + \frac{1}{\Gamma(\kappa)}\int_0^t (t-\nu)^{\kappa-1} K_6(\nu, R(\nu))d\nu,\\
V(t) &= V(0) + \frac{1}{\Gamma(\kappa)}\int_0^t (t-\nu)^{\kappa-1} K_7(\nu, V(\nu))d\nu.
\end{aligned} \tag{26}$$

The kernels are obtained as follows,

$$\begin{aligned}
K_1(t, S(t)) &= \Lambda^\kappa - \frac{\beta^\kappa S(I + \eta_1^\kappa A + \eta_2^\kappa T)}{N} - (\mu^\kappa + \tau^\kappa)S,\\
K_2(t, E(t)) &= (1 - \omega_1^\kappa - \omega_2^\kappa)\frac{\beta^\kappa S(I + \eta_1^\kappa A + \eta_2^\kappa T)}{N} - (\alpha^\kappa + \mu^\kappa)E + \varepsilon^\kappa R,\\
K_3(t, A(t)) &= \omega_1^\kappa \frac{\beta^\kappa S(I + \eta_1^\kappa A + \eta_2^\kappa T)}{N} - (\gamma_1^\kappa + \gamma_2^\kappa + \delta^\kappa + \mu^\kappa)A + \rho^\kappa \alpha^\kappa E,\\
K_4(t, I(t)) &= \omega_2^\kappa \frac{\beta^\kappa S(I + \eta_1^\kappa A + \eta_2^\kappa T)}{N} + (1 - \rho^\kappa)\alpha^\kappa E + \sigma^\kappa \gamma_2^\kappa A - (\theta^\kappa + \delta^\kappa + \mu^\kappa)I,\\
K_5(t, T(t)) &= (1 - \sigma^\kappa)\gamma_2^\kappa A + \theta^\kappa I - (\mu^\kappa + \phi^\kappa)T,\\
K_6(t, R(t)) &= \gamma_1^\kappa A - (\varepsilon^\kappa + \mu^\kappa)R + \psi^\kappa V + \phi^\kappa T,\\
K_7(t, V(t)) &= \tau^\kappa S - (\psi^\kappa + \mu^\kappa)V.
\end{aligned} \tag{27}$$

All the equations in eq. (27) satisfy the Lipschitz conditions with all the compartments having the upper limit. Suppose the functions $S(t)$ and $S^*(t)$ are considered, applying a similar approach for other functions, which gives rise to

$$\|K_1(t, S(t)) - K_1(t, S^*(t))\| = \left\| \frac{1}{N}(\beta^\kappa S(I + \eta_1^\kappa A + \eta_2^\kappa T) + (\mu^\kappa + \tau^\kappa))(S(t) - S^*(t)) \right\|, \tag{28}$$

Let $b_1 = \|\frac{1}{N}(\beta^\kappa S(I + \eta_1^\kappa A + \eta_2^\kappa T) + (\mu^\kappa + \tau^\kappa))\|$. Using a similar approach, the remaining equations are obtained as follows

$$\begin{aligned}
\|K_1(t, S(t)) - K_1(t, S^*(t))\| &= b_1\|(S(t) - S^*(t))\|,\\
\|K_2(t, E(t)) - K_2(t, E^*(t))\| &= b_2\|(E(t) - E^*(t))\|,\\
\|K_3(t, A(t)) - K_3(t, A^*(t))\| &= b_3\|(A(t) - A^*(t))\|,\\
\|K_4(t, I(t)) - K_4(t, I^*(t))\| &= b_4\|(I(t) - I^*(t))\|,\\
\|K_5(t, T(t)) - K_5(t, T^*(t))\| &= b_5\|(T(t) - T^*(t))\|,\\
\|K_6(t, R(t)) - K_6(t, R^*(t))\| &= b_6\|(R(t) - R^*(t))\|,\\
\|K_7(t, V(t)) - K_7(t, V^*(t))\| &= b_7\|(V(t) - V^*(t))\|.
\end{aligned} \tag{29}$$

where $b_1, b_2, b_3, b_4, b_5, b_6$ and b_7 denote the Lipschitz constants, respectively, which correspond to the six kernels and, by this, the Lipschitz condition is satisfied. The algorithm of equations

in eq. (26) can be presented as follows:

$$\begin{aligned}
S_n(t) &= S(0) + \frac{1}{\Gamma(\kappa)}\int_0^t (t-\nu)^{\kappa-1} K_1(\nu, S_{n-1}(\nu))d\nu,\\
E_n(t) &= E(0) + \frac{1}{\Gamma(\kappa)}\int_0^t (t-\nu)^{\kappa-1} K_2(\nu, E_{n-1}(\nu))d\nu,\\
A_n(t) &= A(0) + \frac{1}{\Gamma(\kappa)}\int_0^t (t-\nu)^{\kappa-1} K_3(\nu, A_{n-1}(\nu))d\nu,\\
I_n(t) &= I(0) + \frac{1}{\Gamma(\kappa)}\int_0^t (t-\nu)^{\kappa-1} K_4(\nu, I_{n-1}(\nu))d\nu,\\
T_n(t) &= T(0) + \frac{1}{\Gamma(\kappa)}\int_0^t (t-\nu)^{\kappa-1} K_5(\nu, T_{n-1}(\nu))d\nu,\\
R_n(t) &= R(0) + \frac{1}{\Gamma(\kappa)}\int_0^t (t-\nu)^{\kappa-1} K_6(\nu, R_{n-1}(\nu))d\nu,\\
V_n(t) &= V(0) + \frac{1}{\Gamma(\kappa)}\int_0^t (t-\nu)^{\kappa-1} K_7(\nu, V_{n-1}(\nu))d\nu.
\end{aligned} \tag{30}$$

The form presented below is the successive terms along the initial conditions of the model with their corresponding differences;

$$\begin{aligned}
\Phi_{S,n}(t) &= S_n(t) - S_{n-1}(t)\\
&= \frac{1}{\Gamma(\kappa)}\int_0^t (t-\nu)^{\kappa-1}(K_1(\nu, S_{n-1}(\nu)) - K_1(\nu, S_{n-2}(\nu)))d\nu,\\
\Phi_{E,n}(t) &= E_n(t) - E_{n-1}(t)\\
&= \frac{1}{\Gamma(\kappa)}\int_0^t (t-\nu)^{\kappa-1}(K_2(\nu, E_{n-1}(\nu)) - K_2(\nu, S_{n-2}(\nu)))d\nu,\\
\Phi_{A,n}(t) &= A_n(t) - A_{n-1}(t)\\
&= \frac{1}{\Gamma(\kappa)}\int_0^t (t-\nu)^{\kappa-1}(K_3(\nu, A_{n-1}(\nu)) - K_3(\nu, A_{n-2}(\nu)))d\nu,\\
\Phi_{I,n}(t) &= I_n(t) - I_{n-1}(t)\\
&= \frac{1}{\Gamma(\kappa)}\int_0^t (t-\nu)^{\kappa-1}(K_4(\nu, I_{n-1}(\nu)) - K_4(\nu, I_{n-2}(\nu)))d\nu,\\
\Phi_{T,n}(t) &= T_n(t) - T_{n-1}(t)\\
&= \frac{1}{\Gamma(\kappa)}\int_0^t (t-\nu)^{\kappa-1}(K_5(\nu, T_{n-1}(\nu)) - K_5(\nu, T_{n-2}(\nu)))d\nu,\\
\Phi_{R,n}(t) &= R_n(t) - R_{n-1}(t)\\
&= \frac{1}{\Gamma(\kappa)}\int_0^t (t-\nu)^{\kappa-1}(K_6(\nu, R_{n-1}(\nu)) - K_6(\nu, R_{n-2}(\nu)))d\nu,\\
\Phi_{V,n}(t) &= V_n(t) - V_{n-1}(t)\\
&= \frac{1}{\Gamma(\kappa)}\int_0^t (t-\nu)^{\kappa-1}(K_7(\nu, V_{n-1}(\nu)) - K_7(\nu, V_{n-2}(\nu)))d\nu.
\end{aligned} \tag{31}$$

It is noticed that,

$$\begin{array}{llll}
S_n(t) = \sum_{j=0}^n \Phi_{S,j}(t), & E_n(t) = \sum_{j=0}^n \Phi_{E,j}(t),\\
A_n(t) = \sum_{j=0}^n \Phi_{A,j}(t), & I_n(t) = \sum_{j=0}^n \Phi_{I,j}(t),\\
T_n(t) = \sum_{j=0}^n \Phi_{T,j}(t), & R_n(t) = \sum_{j=0}^n \Phi_{R,j}(t),\\
V_n(t) = \sum_{j=0}^n \Phi_{V,j}(t).
\end{array}$$

Now, we consider that;

$$\begin{aligned}
\Phi_{S,n-1}(t) &= S_{n-1}(t) - S_{n-2}(t),\\
\Phi_{E,n-1}(t) &= E_{n-1}(t) - E_{n-2}(t),\\
\Phi_{A,n-1}(t) &= A_{n-1}(t) - A_{n-2}(t),\\
\Phi_{I,n-1}(t) &= I_{n-1}(t) - I_{n-2}(t),\\
\Phi_{T,n-1}(t) &= T_{n-1}(t) - T_{n-2}(t),\\
\Phi_{R,n-1}(t) &= R_{n-1}(t) - R_{n-2}(t),\\
\Phi_{V,n-1}(t) &= V_{n-1}(t) - V_{n-2}(t).
\end{aligned}$$

We obtained form eq. (31),

$$\begin{aligned}
\|\Phi_{S,n}(t)\| &\leq \frac{1}{\Gamma(\kappa)} b_1 \int_0^t (t-\nu)^{\kappa-1}\|\Phi_{S,n-1}(\nu)\|d\nu,\\
\|\Phi_{E,n}(t)\| &\leq \frac{1}{\Gamma(\kappa)} b_2 \int_0^t (t-\nu)^{\kappa-1}\|\Phi_{E,n-1}(\nu)\|d\nu,\\
\|\Phi_{A,n}(t)\| &\leq \frac{1}{\Gamma(\kappa)} b_3 \int_0^t (t-\nu)^{\kappa-1}\|\Phi_{A,n-1}(\nu)\|d\nu,\\
\|\Phi_{I,n}(t)\| &\leq \frac{1}{\Gamma(\kappa)} b_4 \int_0^t (t-\nu)^{\kappa-1}\|\Phi_{I,n-1}(\nu)\|d\nu,\\
\|\Phi_{T,n}(t)\| &\leq \frac{1}{\Gamma(\kappa)} b_5 \int_0^t (t-\nu)^{\kappa-1}\|\Phi_{T,n-1}(\nu)\|d\nu,\\
\|\Phi_{R,n}(t)\| &\leq \frac{1}{\Gamma(\kappa)} b_6 \int_0^t (t-\nu)^{\kappa-1}\|\Phi_{R,n-1}(\nu)\|d\nu,\\
\|\Phi_{V,n}(t)\| &\leq \frac{1}{\Gamma(\kappa)} b_7 \int_0^t (t-\nu)^{\kappa-1}\|\Phi_{V,n-1}(\nu)\|d\nu.
\end{aligned} \tag{32}$$

Hence, all the model variables depict the bounded functions and the representation of the kernels satisfies the Lipschitz condition. □

Theorem 4. *The Caputo COVID-19 model stated by model (20) has a unique solution for all value of t, such that $t \in [0, a]$ if*

$$\frac{1}{\Gamma(\kappa)} g_{jm} < 1, j = 1, ..., 7 \tag{33}$$

Proof. From the above theorem, one will notice that all the model variables depict the bounded functions and the expressions of the kernels satisfy the Lipschitz condition. Applying the recursive principle on eq. (33) with respect to the model (20), the model is obtained:

$$\begin{aligned}
\|\Phi_{S,n}(t)\| &\leq \|S_0(t)\| \left(\frac{m}{\Gamma(\kappa)} b_1\right)^n,\\
\|\Phi_{E,n}(t)\| &\leq \|E_0(t)\| \left(\frac{m}{\Gamma(\kappa)} b_2\right)^n,\\
\|\Phi_{A,n}(t)\| &\leq \|A_0(t)\| \left(\frac{m}{\Gamma(\kappa)} b_3\right)^n,\\
\|\Phi_{I,n}(t)\| &\leq \|I_0(t)\| \left(\frac{m}{\Gamma(\kappa)} b_4\right)^n,\\
\|\Phi_{T,n}(t)\| &\leq \|T_0(t)\| \left(\frac{m}{\Gamma(\kappa)} b_5\right)^n,\\
\|\Phi_{R,n}(t)\| &\leq \|R_0(t)\| \left(\frac{m}{\Gamma(\kappa)} b_6\right)^n,\\
\|\Phi_{V,n}(t)\| &\leq \|V_0(t)\| \left(\frac{m}{\Gamma(\kappa)} b_7\right)^n.
\end{aligned}$$

Hence, the progression exist and satisfies the conditions describes $\|\Phi_{S,n}(t)\| \longrightarrow 0$, $\|\Phi_{E,n}(t)\| \longrightarrow 0$, $\|\Phi_{A,n}(t)\| \longrightarrow 0$, $\|\Phi_{I,n}(t)\| \longrightarrow 0$, $\|\Phi_{T,n}(t)\| \longrightarrow 0$, $\|\Phi_{R,n}(t)\| \longrightarrow 0$, and $\|\Phi_{V,n}(t)\| \longrightarrow 0$, as $n \longrightarrow \infty$.

$$\|S_{n+1}(t) - S_n(t)\| \leq \sum_{n+1}^{j=n+1} Z_1^j = \frac{Z_1^{n+1} - Z_1^{n+b+1}}{1 - Z_1},$$
$$\|E_{n+1}(t) - E_n(t)\| \leq \sum_{n+1}^{j=n+1} Z_2^j = \frac{Z_1^{n+1} - Z_2^{n+b+1}}{1 - Z_2},$$
$$\|A_{n+1}(t) - A_n(t)\| \leq \sum_{n+1}^{j=n+1} Z_3^j = \frac{Z_1^{n+1} - Z_3^{n+b+1}}{1 - Z_3},$$
$$\|I_{n+1}(t) - I_n(t)\| \leq \sum_{n+1}^{j=n+1} Z_4^j = \frac{Z_1^{n+1} - Z_4^{n+b+1}}{1 - Z_4},$$
$$\|T_{n+1}(t) - T_n(t)\| \leq \sum_{n+1}^{j=n+1} Z_5^j = \frac{Z_1^{n+1} - Z_5^{n+b+1}}{1 - Z_5},$$
$$\|R_{n+1}(t) - R_n(t)\| \leq \sum_{n+1}^{j=n+1} Z_6^j = \frac{Z_1^{n+1} - Z_6^{n+b+1}}{1 - Z_6},$$
$$\|V_{n+1}(t) - V_n(t)\| \leq \sum_{n+1}^{j=n+1} Z_7^j = \frac{Z_1^{n+1} - Z_7^{n+b+1}}{1 - Z_7}.$$

So by hypothesis, $\frac{1}{\Gamma(\kappa)} b_{jm} < 1$, and $S_n, E_n, A_n, I_n, T_n, R_n, V_n$ is the Cauchy progression. By this, the complete desired result for the model (20) is obtained. □

5.4. Iterative solution and stability analysis

The subsequent hypothesis and solutions have been furnished to stabilize the outcome of this proposed model (20)

Theorem 5. *Let $(\mathcal{B}, \|.\|)$ indicate a Banach space and X^* define a self-map on $\mathcal{B}$. In addition, $z_{n+1} = x(X^*, z_n)$ exhibits the recursive expression while $\mathcal{C}(X^*)$ implies the fixed point set on X^* indicating the fixed point set on X^*. Also, by defining such that $\|y^*_{n+1} - x(X^*, y^*_n)\|$ such that $\{y^*_n \subseteq \mathcal{B}\}$. Then, in the iterative approach, $y_{n+1} = x(X^*, y_n)$, X^* is stable if $\lim_{n\longrightarrow\infty} C_n = 0$, that is, $\lim_{n\longrightarrow\infty} C^*_n = p^*$ for $z_{n+1} = X^*$ where n is regarded as the Picard iteration, then the X^* iteration is stable. The hypothesis can be condensed as follows. Let $(\mathcal{B}, \|.\|)$ define a Banach space and X^* be a self-map on $\mathcal{B}$, then for all $x, y \in \mathcal{B}$, we have*

$$S_{n+1}(t) = S_n(t) + \mathcal{L}^{-1}\left\{\frac{1}{S^a}\mathcal{L}\left\{\Lambda^\kappa - \frac{\beta^\kappa S(I + \eta_1^\kappa A + \eta_2^\kappa T)}{N} - (\mu^\kappa + \tau^\kappa)S\right\}\right\},$$
$$E_{n+1}(t) = E_n(t) + \mathcal{L}^{-1}\left\{\frac{1}{S^a}\mathcal{L}\left\{-(\alpha^\kappa + \mu^\kappa)E + \varepsilon^\kappa R + (1 - \omega_1^\kappa - \omega_2^\kappa)\frac{\beta^\kappa S(I + \eta_1^\kappa A + \eta_2^\kappa T)}{N}\right\}\right\},$$
$$A_{n+1}(t) = A_n(t) + \mathcal{L}^{-1}\left\{\frac{1}{S^a}\mathcal{L}\left\{\omega_1^\kappa \frac{\beta^\kappa S(I + \eta_1^\kappa A + \eta_2^\kappa T)}{N} - (\gamma_1^\kappa + \gamma_2^\kappa + \delta^\kappa + \mu^\kappa)A + \rho^\kappa \alpha^\kappa E\right\}\right\},$$
$$I_{n+1}(t) = I_n(t) + \mathcal{L}^{-1}\left\{\frac{1}{S^a}\mathcal{L}\left\{\omega_2^\kappa \frac{\beta^\kappa S(I + \eta_1^\kappa A + \eta_2^\kappa T)}{N} + (1 - \rho^\kappa)\alpha^\kappa E + \sigma^\kappa \gamma_2^\kappa A - (\theta^\kappa + \delta^\kappa + \mu^\kappa)I\right\}\right\},$$
$$T_{n+1}(t) = T_n(t) + \mathcal{L}^{-1}\left\{\frac{1}{S^a}\mathcal{L}\left\{(1 - \sigma^\kappa)\gamma_2^\kappa A + \theta^\kappa I - (\mu^\kappa + \phi^\kappa)T\right\}\right\},$$
$$R_{n+1}(t) = R_n(t) + \mathcal{L}^{-1}\left\{\frac{1}{S^a}\mathcal{L}\left\{\gamma_1^\kappa A - (\varepsilon^\kappa + \mu^\kappa)R + \psi^\kappa V + \phi^\kappa T\right\}\right\},$$
$$V_{n+1}(t) = V_n(t) + \mathcal{L}^{-1}\left\{\frac{1}{S^a}\mathcal{L}\left\{\tau^\kappa S - (\psi^\kappa + \mu^\kappa)V\right\}\right\}. \tag{34}$$

Suppose $\mathcal{X}$ is defined as a self-map, and the following results are obtained:
Let $T_0 = \mu^\kappa + \tau^\kappa, T_1 = \alpha^\kappa + \mu^\kappa, T_2 = \gamma_1^\kappa + \gamma_2^\kappa + \delta^\kappa + \mu^\kappa, T_3 = (\theta^\kappa + \delta^\kappa + \mu^\kappa), T_4 = \mu^\kappa + \phi^\kappa, T_5 = \varepsilon^\kappa + \mu^\kappa$.

$$\begin{aligned}
\mathcal{X}[S_n(t)] &= S_{n+1}(t) \\
&= S_n(t) + \mathcal{L}^{-1}\left\{\frac{1}{S^a}\mathcal{L}\left\{\Lambda^\kappa - \frac{\beta^\kappa S(I + \eta_1^\kappa A + \eta_2^\kappa T)}{N} - T_0 S\right\}\right\}, \\
\mathcal{X}[E_n(t)] &= E_{n+1}(t) \\
&= E_n(t) + \mathcal{L}^{-1}\left\{\frac{1}{S^a}\mathcal{L}\left\{-T_1 E + \varepsilon^\kappa R + (1 - \omega_1^\kappa - \omega_2^\kappa)\frac{\beta^\kappa S(I + \eta_1^\kappa A + \eta_2^\kappa T)}{N}\right\}\right\}, \\
\mathcal{X}[A_n(t)] &= A_{n+1}(t) \\
&= A_n(t) + \mathcal{L}^{-1}\left\{\frac{1}{S^a}\mathcal{L}\left\{\omega_1^\kappa \frac{\beta^\kappa S(I + \eta_1^\kappa A + \eta_2^\kappa T)}{N} - T_2 A + \rho^\kappa \alpha^\kappa E\right\}\right\}, \\
\mathcal{X}[I_n(t)] &= I_{n+1}(t) \\
&= I_n(t) + \mathcal{L}^{-1}\left\{\frac{1}{S^a}\mathcal{L}\left\{\omega_2^\kappa \frac{\beta^\kappa S(I + \eta_1^\kappa A + \eta_2^\kappa T)}{N} + (1 - \rho^\kappa)\alpha^\kappa E + \sigma^\kappa \gamma_2^\kappa A - T_3 I\right\}\right\}, \\
\mathcal{X}[T_n(t)] &= T_{n+1}(t) \\
&= T_n(t) + \mathcal{L}^{-1}\left\{\frac{1}{S^a}\mathcal{L}\left\{(1 - \sigma^\kappa)\gamma_2^\kappa A + \theta^\kappa I - T_4 T\right\}\right\}, \\
\mathcal{X}[R_n(t)] &= R_{n+1}(t) \\
&= R_n(t) + \mathcal{L}^{-1}\left\{\frac{1}{S^a}\mathcal{L}\left\{\gamma_1^\kappa A - T_5 R + \psi^\kappa V + \phi^\kappa T\right\}\right\}, \\
\mathcal{X}[V_n(t)] &= V_{n+1}(t) \\
&= V_n(t) + \mathcal{L}^{-1}\left\{\frac{1}{S^a}\mathcal{L}\left\{\tau^\kappa S - (\psi^\kappa + \mu^\kappa)V\right\}\right\}.
\end{aligned} \tag{35}$$

$\mathcal{X}$ is stable if the following conditions are satisfied

$$
\begin{aligned}
1 &> \{1-\Lambda^{\kappa}-\beta^{\kappa}(Q_1+Q_2+Q_3)f_1-\beta^{\kappa}(Q_1+Q_2\\
&\quad +Q_3)f_2-T_0K_1\},\\
1 &> \{1-(1-\omega_1^{\kappa}-\omega_2^{\kappa})\beta^{\kappa}(Q_1+Q_2+Q_3)f_1-(1-\omega_1^{\kappa}\\
&\quad -\omega_2^{\kappa})\beta^{\kappa}(Q_1+Q_2+Q_3)f_2-(\varepsilon^{\kappa}+T_1)K_2\},\\
1 &> \{1-\omega_1^{\kappa}\beta^{\kappa}(Q_1+Q_2+Q_3)f_1-\omega_1^{\kappa}\beta^{\kappa}(Q_1+Q_2+Q_3)f_2-\\
&\quad (\rho^{\kappa}\alpha^{\kappa}+T_2)K_3\},\\
1 &> \{1-\omega_2^{\kappa}\beta^{\kappa}(Q_1+Q_2+Q_3)f_1-\omega_2^{\kappa}\beta^{\kappa}(Q_1+Q_2+Q_3)f_2\\
&\quad -((1-\rho^{\kappa})\alpha^{\kappa}+\sigma^{\kappa}\gamma^{\kappa}+T_3)K_4\},\\
1 &> \{1-((1-\sigma^{\kappa})\gamma_2^{\kappa}+\theta^{\kappa}+T_4)k_5\},\\
1 &> \{1-(\gamma_1^{\kappa}+T_5+\psi^{\kappa}+\phi^{\kappa})k_6\},\\
1 &> \{1-(\tau^{\kappa}-(\psi^{\kappa}+\mu^{\kappa}))k_7\}.
\end{aligned}
$$

Proof. The following equations were obtained when evaluated around the map $\mathcal{X}$ which is a fixed point,

$$
\begin{aligned}
\mathcal{X}[S_n(t)]-\mathcal{X}[S_m(t)] &= S_n(t)-S_m(t),\\
\mathcal{X}[E_n(t)]-\mathcal{X}[E_m(t)] &= E_n(t)-E_m(t),\\
\mathcal{X}[A_n(t)]-\mathcal{X}[A_m(t)] &= A_n(t)-A_m(t),\\
\mathcal{X}[I_n(t)]-\mathcal{X}[I_m(t)] &= I_n(t)-I_m(t),\\
\mathcal{X}[T_n(t)]-\mathcal{X}[T_m(t)] &= T_n(t)-T_m(t),\\
\mathcal{X}[R_n(t)]-\mathcal{X}[R_m(t)] &= R_n(t)-R_m(t),\\
\mathcal{X}[V_n(t)]-\mathcal{X}[V_m(t)] &= V_n(t)-V_m(t).
\end{aligned}
\tag{36}
$$

Taking the norm of both sides of the above equation

$$
\begin{aligned}
\|\mathcal{X}[S_n(t)]-\mathcal{X}[S_m(t)]\| = \Big\|&\mathcal{L}^{-1}\Big\{\frac{1}{S^a}\mathcal{L}\Big\{\Lambda^{\kappa}-l_1-T_0S_n\Big\}\Big\}\\
&-\mathcal{L}^{-1}\Big\{\frac{1}{S^a}\mathcal{L}\{\Lambda^{\kappa}-l_2\\
&-T_0S_m\}\Big\}S_n(t)-S_m(t)\Big\|,
\end{aligned}
\tag{37}
$$

where

$$
\begin{aligned}
l_1 &= \frac{\beta^{\kappa}S_n(I_n+\eta_1^{\kappa}A_n+\eta_2^{\kappa}T_n)}{N},\\
l_2 &= \frac{\beta^{\kappa}S_m(I_m+\eta_1^{\kappa}A_m+\eta_2^{\kappa}T_m)}{N}.
\end{aligned}
$$

Further simplification of eq. (37), leads;

$$
\begin{aligned}
\|\mathcal{X}[S_n(t)]-\mathcal{X}[S_m(t)]\| \le \|S_n(t)-S_m(t)\| &+ \mathcal{L}^{-1}\Big\{\frac{1}{S^a}\mathcal{L}\\
&+\|\beta^{\kappa}(S_nI_n-S_mI_m)\|\frac{1}{N}\\
&+\|\beta^{\kappa}\eta_1^{\kappa}(S_nA_n-S_mA_m)\|\frac{1}{N}\\
&+\|\beta^{\kappa}\eta_2^{\kappa}(S_nT_n-S_mT_m)\|\frac{1}{N}\\
&-\|T_0(S_n-S_m)\|\Big\}.
\end{aligned}
\tag{38}
$$

Using these assumptions,

$$
\begin{aligned}
\|E_n(t)-E_m(t)\| &\cong \|S_n(t)-S_m(t)\|,\\
\|A_n(t)-A_m(t)\| &\cong \|S_n(t)-S_m(t)\|,\\
\|I_n(t)-I_m(t)\| &\cong \|S_n(t)-S_m(t)\|,\\
\|T_n(t)-T_m(t)\| &\cong \|S_n(t)-S_m(t)\|,\\
\|R_n(t)-R_m(t)\| &\cong \|S_n(t)-S_m(t)\|,\\
\|V_n(t)-V_m(t)\| &\cong \|S_n(t)-S_m(t)\|,
\end{aligned}
\tag{39}
$$

after putting the above relation, leads

$$
\begin{aligned}
\|\mathcal{X}[S_n(t)]-\mathcal{X}[S_m(t)]\| \le \|S_n(t)-S_m(t)\| &+ \mathcal{L}^{-1}\Big\{\frac{1}{S^a}\mathcal{L}\\
&+\|\beta^{\kappa}(S_nI_n-S_mI_m)\|\frac{1}{N}\\
&+\|\beta^{\kappa}\eta_1^{\kappa}(S_nA_n-S_mA_m)\|\frac{1}{N}\\
&+\|\beta^{\kappa}\eta_2^{\kappa}(S_nT_n-S_mT_m)\|\frac{1}{N}\\
&-\|T_0(S_n-S_m)\|\Big\}.
\end{aligned}
\tag{40}
$$

Since the progressions $S_m(t)$, $E_m(t)$, $A_m(t)$, $I_m(t)$, $T_m(t)$, $R_m(t)$, $V_m(t)$ are convergent and bounded, their exist seven different constant $S_1>0$, $S_2>0$, $S_3>0$, $S_4>0$, $S_5>0$, $S_6>0$ and $S_7>0$ for all t. Then $\| S_m(t) \|<\| S_1 \|$, $\| E_m(t) \|<\| S_2 \|$, $\| A_m(t) \|<\| S_3 \|$, $\| I_m(t) \|<\| S_4 \|$, $\| T_m(t) \|<\| S_5 \|$, $\| R_n(t) \|<\| S_6 \|$, $\| V_n(t) \|<\| S_7 \|$, $(m,n)\in\mathbb{N}\times\mathbb{N}$. Through the relation, we can achieve the following.

$$
\begin{aligned}
\|\mathcal{X}[S_n(t)]-\mathcal{X}[S_m(t)]\| &\le \|S_n(t)-S_m(t)\|\{1-\Lambda^{\kappa}-\beta^{\kappa}(Q_1\\
&\quad +Q_2+Q_3)f_1-\beta^{\kappa}(Q_1+Q_2\\
&\quad +Q_3)f_2-T_0K_1\},\\
\|\mathcal{X}[E_n(t)]-\mathcal{X}[E_m(t)]\| &\le \|E_n(t)-E_m(t)\|\{1-(1-\omega_1^{\kappa}\\
&\quad -\omega_2^{\kappa})\beta^{\kappa}(Q_1+Q_2+Q_3)f_1-(1\\
&\quad -\omega_1^{\kappa}-\omega_2^{\kappa})\beta^{\kappa}(Q_1+Q_2\}+Q_3)f_2\\
&\quad -\{(\varepsilon^{\kappa}+T_1)K_2\}\},\\
\|\mathcal{X}[A_n(t)]-\mathcal{X}[A_m(t)]\| &\le \|A_n(t)-A_m(t)\|\{1-\omega_1^{\kappa}\beta^{\kappa}(Q_1\\
&\quad +Q_2+Q_3)f_1-\omega_1^{\kappa}\beta^{\kappa}(Q_1+Q_2\\
&\quad +Q_3)f_2-(\rho^{\kappa}\alpha^{\kappa}+T_2)K_3\},\\
\|\mathcal{X}[I_n(t)]-\mathcal{X}[I_m(t)]\| &\le \|I_n(t)-I_m(t)\|\{1-\omega_2^{\kappa}\beta^{\kappa}(Q_1\\
&\quad +Q_2+Q_3)f_1-\omega_2^{\kappa}\beta^{\kappa}(Q_1+Q_2\\
&\quad +Q_3)f_2-((1-\rho^{\kappa})\alpha^{\kappa}+\sigma^{\kappa}\gamma^{\kappa}\}\\
&\quad +T_3)K_4,\\
\|\mathcal{X}[T_n(t)]-\mathcal{X}[T_m(t)]\| &\le \|T_n(t)-T_m(t)\|\{1-((1-\sigma^{\kappa})\gamma_2^{\kappa}\\
&\quad +\theta^{\kappa}+T_4)k_5\},\\
\|\mathcal{X}[R_n(t)]-\mathcal{X}[R_m(t)]\| &\le \|R_n(t)-R_m(t)\|\{1-(\gamma_1^{\kappa}+T_5\\
&\quad +\psi^{\kappa}+\phi^{\kappa})k_6\},\\
\|\mathcal{X}[V_n(t)]-\mathcal{X}[V_m(t)]\| &\le \|lV_n(t)-V_m(t)\|\{1-(\tau^{\kappa}-(\psi^{\kappa}\\
&\quad +\mu^{\kappa}))k_7\}.
\end{aligned}
\tag{41}
$$

Hence, the proof is complete. □

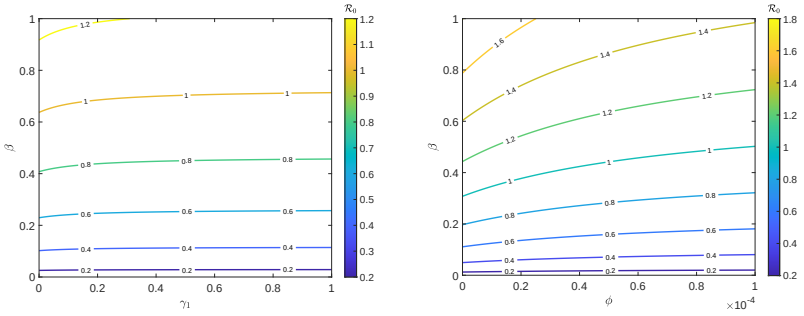

(a) Contour plot of $\mathcal{R}_0$ as a function of β and γ_1

(b) Contour plot of $\mathcal{R}_0$ as a function of β and ϕ

(c) Contour plot of $\mathcal{R}_0$ as a function of β and θ

(d) Contour plot of $\mathcal{R}_0$ as a function of θ and τ

Figure 3. 2-D contour plots of the control reproduction number, $\mathcal{R}_0$

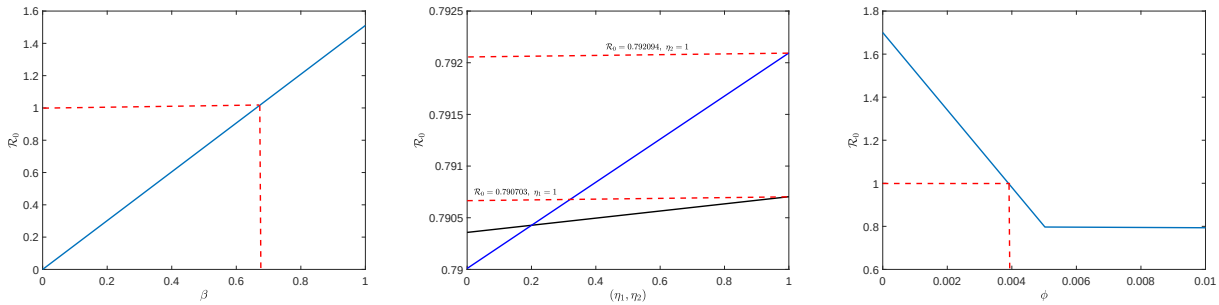

(a) Relationship between $\mathcal{R}_0$ and β

(b) Relationship between $\mathcal{R}_0$ and (η_1, η_2)

(c) Relationship between $\mathcal{R}_0$ and ϕ

Figure 4. Simulations showing the relationship between the control reproduction number and sensitive parameters of model (2)

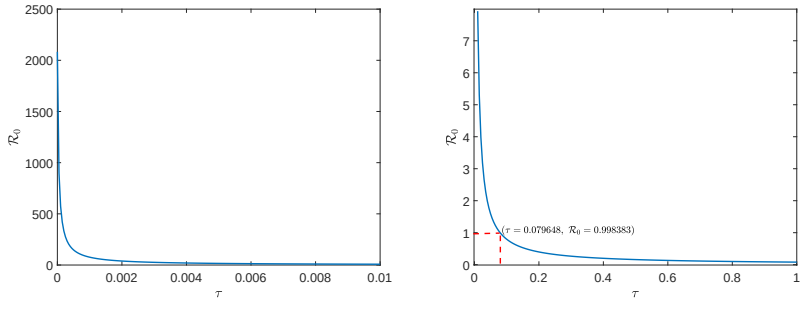

(a)

(b)

Figure 5. Simulations showing the relationship between the control reproduction number, $\mathcal{R}_0$, and the vaccination rate, τ

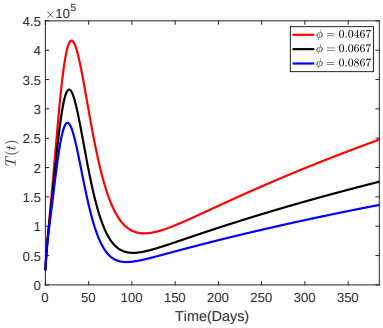

Figure 6. Time series of treated compartment for different values of recovery rate for treated humans ϕ

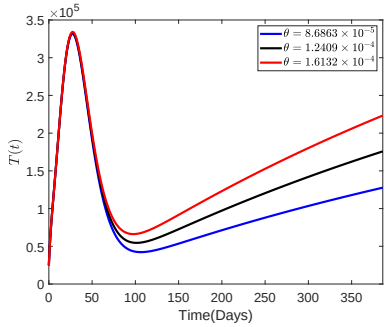

(a) Treated humans with effects of treatment rate for symptomatic infectious humans θ

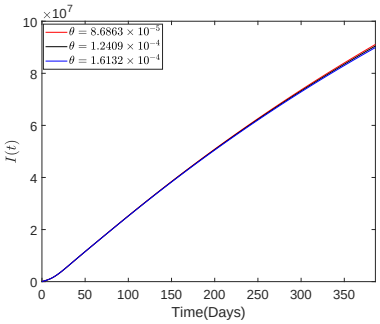

(b) Symptomatic humans with effects of treatment rate for symptomatic infectious humans θ

Figure 7. Time series of compartments of model (2) for different values of treatment rate for symptomatic infectious humans θ

6. Numerical simulations and discussion

6.1. Numerical simulations and discussion of autonomous model

Here, the numerical analysis of model (2) is carried out to gain insight into the dynamics of COVID-19 transmission. All simulations are performed in MATLAB with `ode45` routine using the initial data previously estimated in Section 4 as $S(0) = 242753239$, $E(0) = 496720$, $A(0) = 248360$, $I(0) = 24836$, $T(0) = 24836$, $R(0) = 20808$, $V(0) = 30184392$ and the model parameter as provided in Table 2.

6.2. Sensitivity analysis

To assess the parameters that most drive the dynamics of transmission and spread of COVID-19 described by model (2), we conduct a sensitivity analysis of the model by employing the normalized sensitivity index approach as previously used by the authors in [47, 51, 59, 60]. By definition, the normalized forward sensitivity index of the control reproduction number $\mathcal{R}_0$ depends differently on the parameter Ω.

$$S_{\Omega}^{\mathcal{R}_0} = \frac{\partial \mathcal{R}_0}{\partial \Omega} \times \frac{\Omega}{\mathcal{R}_0},$$

where Ω is considered as any parameter of the control reproduction number $\mathcal{R}_0$. In particular, the analytical sensitivity indices of the control reproduction number $\mathcal{R}_0$ with respect to the effective transmission coefficient β and the vaccination rate τ are calculated as

$$S_{\beta}^{\mathcal{R}_0} = \frac{\partial \mathcal{R}_0}{\partial \beta} \times \frac{\beta}{\mathcal{R}_0} = +1,$$

$$S_{\tau}^{\mathcal{R}_0} = \frac{\partial \mathcal{R}_0}{\partial \tau} \times \frac{\tau}{\mathcal{R}_0} = -\frac{\tau}{\tau + \mu}.$$

Similarly, the analytical sensitivity indices for $\mathcal{R}_0$ with respect to the other parameters of model (2) defining it are computed but not reported in this paper because the results are complex. Meanwhile, the numerical sensitivity indices of all parameters are obtained using the baseline parameter values presented in Table 2. The results are summarized in Table 3.

Table 3. Sensitivity analysis of model (2) with respect to $\mathcal{R}_0$.

Parameter	Sensitivity index	Parameter	Sensitivity index
β	$+1.0000000000$	τ	-0.9996204195
μ	$+0.7751419783$	θ	-0.7281082155
σ	$+0.0890230505$	ω_1	-0.4759456452
γ_2	$+0.0268808923$	δ	-0.0467307702
η_2	$+0.0006593445$	γ_1	-0.0270805785
η_1	$+0.0002184361$	ϕ	-0.0006589675
α	$+0.0001760801$	ρ	-0.0000319173
ω_2	$+0.0000056105$		

Table 3 shows that the model parameters are categorized into two according to the sign of their sensitivity indices. The sensitivity index is positive for some parameters (β, μ, σ, γ_2, η_1, η_2, α, and ω_2), while it is negative for the others (τ, θ, ω_1, δ, γ_1, ϕ, and ρ). The epidemiological implication of the positive sign of the sensitivity index of the control reproduction number to the model parameters is that the control reproduction number will increase when the value of any of the parameters in this category is increased and will decrease when the value of any of the

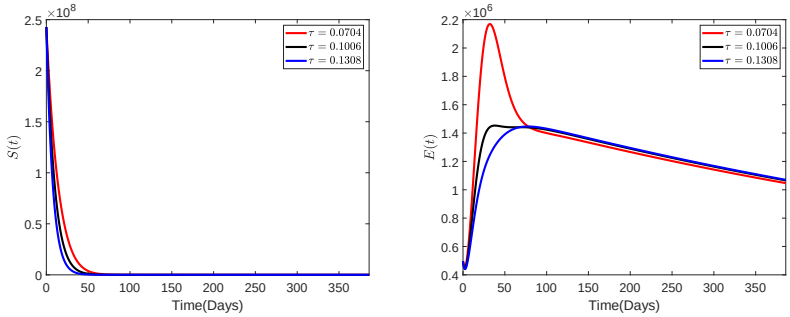

(a) Susceptible humans with effects of vaccination rate τ

(b) Exposed humans with effects of vaccination rate τ

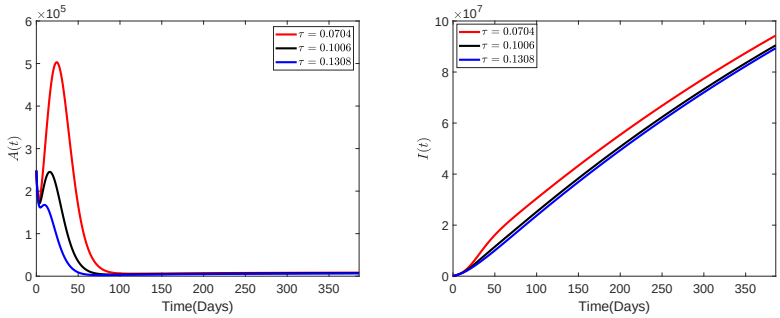

(c) Asymptomatic humans with effects of vaccination rate τ

(d) Symptomatic humans with effects of vaccination rate τ.

Figure 8. Time series of the compartments S, E, A and I for different values of vaccination rate τ

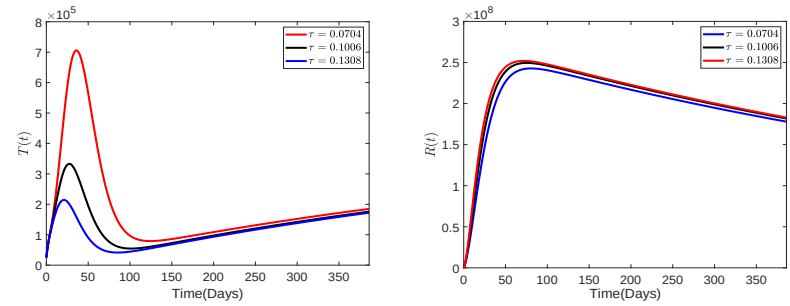

(a) Treated humans with effects of vaccination rate τ

(b) Recovered humans with effects of vaccination rate τ

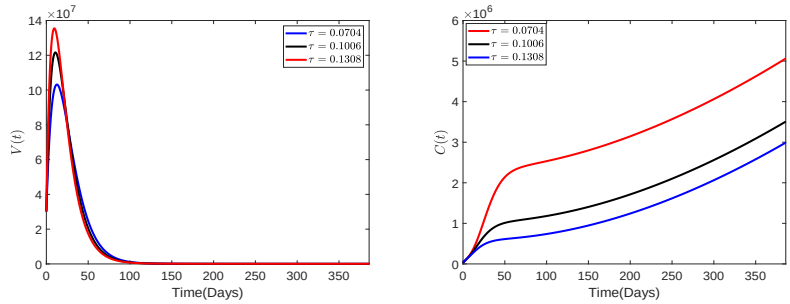

(c) Vaccinated humans with effects of vaccination rate τ

(d) Cumulative number of infected humans with effects of vaccination rate τ

Figure 9. Time series of the compartments of model (2) for different values of vaccination rate τ.

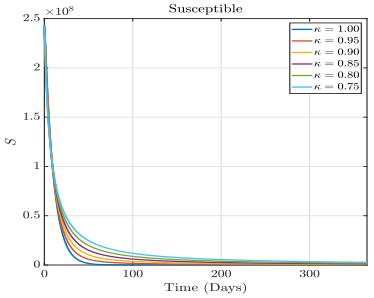

(a) Effect of fractional on the susceptible compartment, $S(t)$.

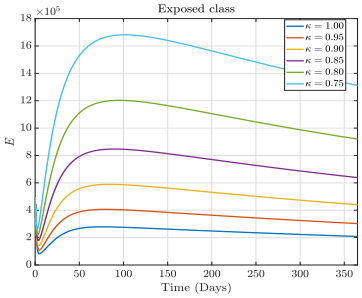

(b) Effect of fractional on the exposed compartment, $E(t)$.

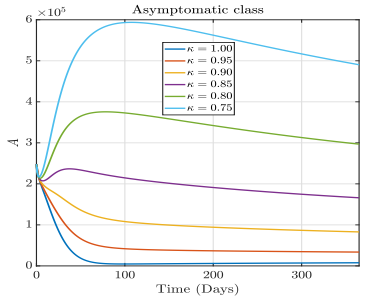

(c) Effect of fractional on the asymptomatic compartment, $A(t)$.

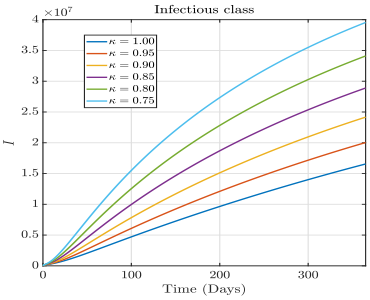

(d) Effect of fractional on the symptomatic compartment, $I(t)$.

Figure 10. Effect of memory on the $S(t), E(t), A(t)$, and $I(t)$, respectively. Considering $\kappa \in [0.75 : 0.5 : 1.00]$

parameters in this set is reduced. For example, the epidemiological implication of $S_\beta^{\mathcal{R}_0} = +1$ is that increasing or decreasing the transmission rate β by 1% will increase or decrease the number of control reproduction $\mathcal{R}_0$ by 1%. However, the control reproduction number will decrease with an increase in the value of any of the parameters with respect to which the sensitivity index of the control reproduction number is negative. A decrease in the value of any of the parameters will increase the value of the control reproduction number $\mathcal{R}_0$. Thus, the sensitivity analysis of the COVID-19 model has provided valuable information about the transmission dynamics of the disease in the host population. In particular, it will help public health authorities and policy makers decide where to put more effort in the fight against the further spread of COVID-19 in the community. We further explore the impacts of the sensitive parameters on the control reproduction number, $\mathcal{R}_0$, and on the compartments of the model (2).

1. Effects of influential parameters on $\mathcal{R}_0$
   Here, we assess the impacts of some key sensitive parameters on the control reproduction number of the COVID-19 model (2).
   To demonstrate how changes in two sensitive parameters affect the control reproduction number, $\mathcal{R}_0$, and in turn affect the community spread of COVID-19 in the population, Figure 3 presents the contour plots of the control reproduction number as a function of two sensitive model parameters. Figures 3a to 3c confirm that it is possible to reduce the control reproduction number below the unity threshold if efforts are made to reduce the transmission rate β while enhancing the recovery rate of asymptotically infected individuals upon case detection, improving the management of treated/hospitalized individuals to ensure quick recovery, and improving the case detection of symptomatic cases for proper treatment or hospitalization. Furthermore, Figure 3d shows that the control reproduction number decreases with an increase in vaccination rate τ and treatment rate for symptomatic infectious people θ.
   In Figure 4, how the potential spread of COVID-19 described by model (2) is driven by the parameters of the model is illustrated. Figure 4a shows that the spread and transmission of COVID-19 will be under control when β is below 0.673367 so that the control reproduction number is below unity. Above this value of β, the control reproduction number increases as the rate of transmission (β) increases. The effects of reduced coronavirus transmission rate from asymptomatic and treated individuals, η_1 and η_2, respectively, on the control reproduction number are shown in Figure 4b. It is observed that when η_1 increases from 0 to 1, the value of the control reproduction number increases from 0.790358 to 0.790703, while the value of the control reproduction number increases from 0.79 to 0.792094 when η_2 increases from 0 to 1. It is deduced that the classical necessary requirement of $\mathcal{R}_0 < 1$ is achieved even when η_1 or η_2 increases from 0 to 1, however, the increase in η_2 increases $\mathcal{R}_0$ toward a more serious global epidemic situation compared to that of η_1. This suggests that personal protective equipment should be strictly used by health professionals when

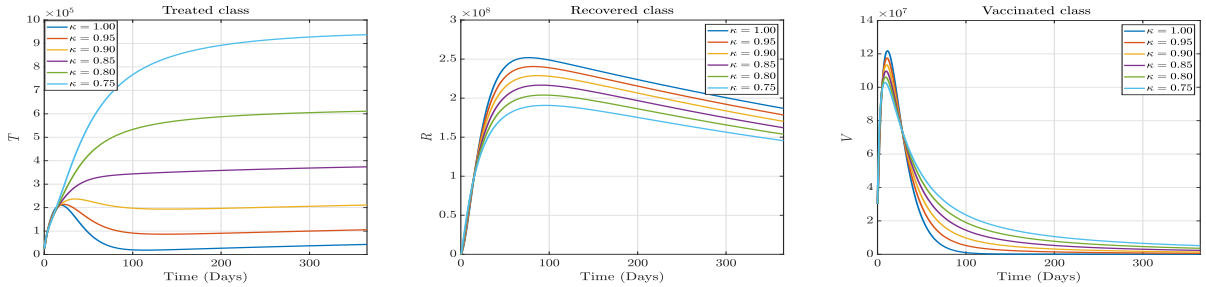

(a) Effect of fractional on the treated compartment, $T(t)$

(b) Effect of fractional on the recovered compartment, $R(t)$

(c) Effect of fractional on the vaccinated compartment, $V(t)$

Figure 11. Effect of Caputo fractional on the $T(t), R(t)$ and $V(t)$, respectively. Considering $\kappa \in [0.75 : 0.5 : 1]$

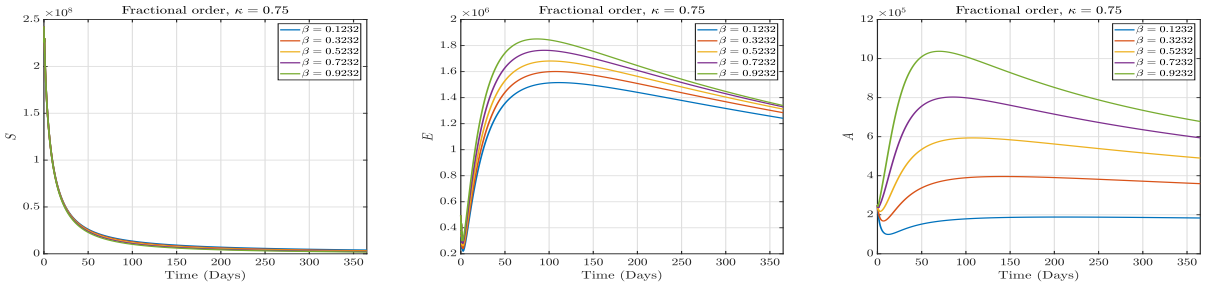

(a) Varying the transmission rate on the susceptibles, $S(t)$.

(b) Varying the transmission rate on the exposed, $E(t)$.

(c) Varying the transmission rate on the asymptomatic, $A(t)$.

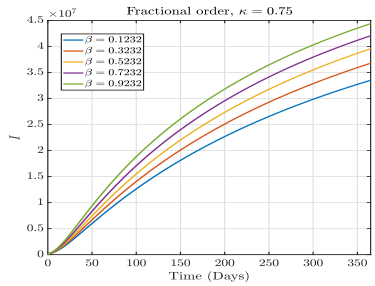

(d) Varying the transmission rate on the symptomatic, $I(t)$.

Figure 12. Effect of varying the transmission rate on the $S(t), E(t), A(t)$, and $I(t)$, respectively. Considering $\kappa = 0.75$

caring for treated or hospitalized people to avoid spreading the virus by treated individuals. In Figure 4c it is shown that when the recovery rate for treated individuals ϕ increases from 0 to 0.0005, the value of the control reproduction number drops from 1.70018 to 0.796876. Above this region, the value of the control reproduction number remains constant at 0.796876 when ϕ increases to 0.01. Generally, the necessary requirement of $\mathcal{R}_0 < 1$ is achieved when the recovery rate is above the value of 0.004, so that the potential spread of the disease is under control.

Figure 5 is presented to evaluate the effectiveness of vaccine uptake in stemming the potential spread of COVID-19 in the population. Specifically, the impact of the vaccination rate, τ, on the control reproduction number, $\mathcal{R}_0$, is assessed. It is observed from Figure 5b that the necessary requirement of $\mathcal{R}_0 < 1$ is achieved when the vaccination rate τ is above a value of 0.079648. However, a slowdown of the vaccination rate from 0.079648 to 0.01 may lead to a serious pandemic situation as the control reproduction number increases from 0.998383 to 7.92548. Moreover, a worsening situation of pandemic is possible when no or almost no effort of vaccination is put in place as the value of control reproduction number becomes very high, as demonstrated in Figure 5a.

Figure 6 demonstrates the effects of recovery rate for treated individuals ϕ on the dynamics of COVID-19 described by model (2). The number of treated individuals

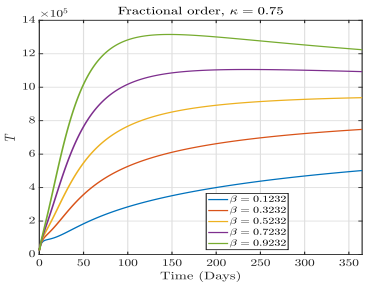

(a) Varying the transmission rate on the treated, $T(t)$

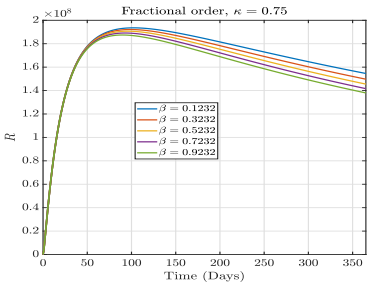

(b) Varying the transmission rate on the recovered, $R(t)$

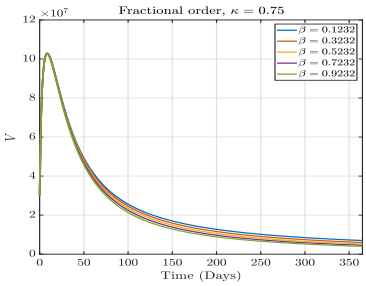

(c) Varying the transmission rate on the vaccinated, $V(t)$

Figure 13. Effect of varying the transmission rate on the $T(t)$, $R(t)$ and $V(t)$, respectively. Considering $\kappa = 0.75$

is shown to decrease as the recovery rate for treated individuals increases and increases when the recovery rate for treated individuals decreases. These, in turn, lead to a respective decrease and increase in the sizes of asymptomatic and symptomatic human sub-populations and the final size of the epidemic at the population level. However, this report omitted these results because they are not very perceptible graphically.

Figure 7 illustrates the effects of treatment rate for symptomatic infectious humans for different values on the dynamics of COVID-19 transmission and spread in the host population. It is confirmed that the number of infectious individuals reduces (see Figure 7b) as more infected people are treated (as shown in Figure 7a). On the other hand, more people are infected when the treatment rate θ is reduced. This suggests that improving efforts to treat infectious people can be helpful in reducing the burden of diseases in the population.

Furthermore, the effects of the vaccination rate τ for different values on the spread dynamics of COVID-19 at the host population level are evaluated as Figure 9 shows. It is observed that when the vaccination rate τ is increased from 0.1006 to 0.1308, the majority of the susceptible individuals are either protected or vaccinated against COVID-19 infection (see Figures 8a and 9c) which in turn leads to fewer number of people at the risk of infection (as shown in Figures 8b to 8d and 9d) and thereby leading to fewer number of people getting treated and recovering from COVID-19 infection as Figures 9a and 9b, respectively, show. However, the case is contrary when τ is reduced from 0.1006 to 0.0704. It is confirmed, as shown in Figure 9 that more people are infected (including asymptomatic and symptomatic infections) as a result of more susceptible individuals who are not protected by not getting vaccinated (or not using non-pharmaceutical protective measures such as face mask, observing social distancing, ensuring good personal hygiene, among others), which consequently leads to more people being treated and recovering from COVID-19 infections. Thus, a high vaccination coverage rate is strongly advised to help overcome the community spread of COVID-19.

6.3. *Fractional numerical simulation*

In this section, we show the vital dynamics of the importance of fractional Caputo derivatives. Figures 10 and 11 show the effect of memory on the $S(t), E(t), A(t),, I(t), T(t), R(t)$, and $V(t)$ compartments, respectively; when the fractional order, $\kappa \in [0.75, 0.80, 0.85, 0.90, 0.95, 1.00]$. Figure 10a shows that a decrease in fractional order indicates that the number of susceptibles slightly moves from the equilibrium point of the model in an integer order. The change in dynamics may be the result of susceptible individuals changing their behaviour toward the disease due to previous occurrences of the disease outbreak. Figures 10b to 10d and 11a show that a drop in fractional order means that the number of people exposed, asymptomatic, symptomatic, and treated moves away from the equilibrium point of the model, which is shown in integer order. The change in dynamics may be the result of exposed, asymptomatic, symptomatic, and treated individuals changing their behaviour toward the disease due to previous occurrences of the disease outbreak. Figure 11b shows that as fractional order reduces, the number of recovered individuals also decreases during the course of disease spread. Figure 11c shows the dynamics of the vaccinated class

when considering the integer model and the fractional model. Figure 11c indicates crisscrossing behaviours during the first 50 days of vaccination implementation in COVID-19 communities. Figures 12 and 13 show the effect of varying the transmission rate in compartments $S(t), E(t), A(t), I(t), T(t), R(t)$ and $V(t)$, respectively. Considering the fractional order, $\kappa = 0.75$. Figures 12a, 13b and 13c show that an increase in the transmission rate reduces the number of susceptible, recovered, and vaccinated individuals when feeding the memory of COVID-19 in communities. Figures 12b to 12d and 13a indicate that an increase in the transmission rate increases the number of exposed, asymptomatic, symptomatic, and treated individuals, respectively.

The memory effect presented in this study, captured by fractional differential operators, significantly enhances the precision of this proposed model by incorporating the long-term effects of past events, which are often observed in the dynamics of real-world diseases. This effect allows this model to better account for the historical context of disease spread, including delayed responses and the accumulated impact of previous outbreaks. As demonstrated in the manuscript, the fractional order introduces a more realistic representation of the population's behaviour over time, reflecting changes in susceptibility, exposure, and recovery based on prior disease experiences. It improves the model's ability to predict future trends and offers a more flexible and precise framework than classical integer-order models, which may overlook such memory-based effects.

The application of fractional differential operators, particularly fractional Caputo derivatives, enhances the epidemiological modeling by incorporating the effects of memory and past occurrences of the disease on the population's dynamics. In the manuscript, Figures 10 and 11 demonstrate how the variation of the fractional order ($\kappa \in [0.75, 0.80, 0.85, 0.90, 0.95, 1.00]$) affects the dynamics of compartments such as $S(t)$, $E(t)$, $A(t)$, $I(t)$, $T(t)$, $R(t)$ and $V(t)$. Specifically, a decrease in fractional order causes a slight deviation of the number of susceptible individuals from the equilibrium, reflecting changes in behaviour due to the memory of past outbreaks, as shown in Figure 10a. Similarly, Figures 10b to 10d and 11a illustrate that the number of exposed, asymptomatic, symptomatic, and treated individuals also deviates from equilibrium in fractional order, which is attributed to changes in behaviour based on prior disease experience. Furthermore, Figure 11b shows that a reduction in fractional order results in fewer recovered individuals over the course of disease spread, further highlighting the importance of memory in disease dynamics. The effect of fractional operators is particularly evident in the vaccination dynamics, where Figure 11c presents the crisscrossing behaviour in the vaccinated class in the fractional model compared to the integer model. This indicates how memory effects in the model can alter the outcomes of vaccination implementation, reflecting a more realistic scenario of disease control in populations with previous exposure.

7. Conclusion

COVID-19, caused by the novel severe acute respiratory syndrome coronavirus 2 (SARS-CoV-2), continues to pose significant challenges to global health and society. In this study, we proposed and analyzed a deterministic compartmental model to capture the dynamics of COVID-19 transmission. We calculated the basic reproduction number, $\mathcal{R}_0$, established the model equilibrium, and used the centre-manifold theorem to demonstrate the existence of bifurcation phenomena. The model was calibrated with publicly available data on cumulative daily cases of COVID-19 in Indonesia from July 1, 2021, to July 21, 2022, to estimate key parameters. A sensitivity analysis identified the most influential parameters in transmission dynamics, including the effective transmission rate (β), the natural mortality rate (μ), the vaccination rate (τ) and the treatment rate for symptomatic infectious individuals (θ).

Further analysis revealed that these critical parameters significantly impact the disease threshold $\mathcal{R}_0$ and the population's disease dynamics, providing valuable insights for formulating effective public health policies. The study highlights the importance of public adherence to preventive measures, such as reducing β, enhancing treatment efforts, and increasing vaccine uptake to control the disease burden and mitigate the severity of future outbreaks in Indonesia.

In addition, we extended the integer-order model to a fractional Caputo model to capture the memory dynamics in disease spread. The existence and uniqueness of the fractional model were established using fixed-point theory, and stability was assessed through iterative solutions. Numerical simulations indicated that a decrease in the fractional order causes deviations from the equilibrium, particularly in susceptible, exposed, asymptomatic, symptomatic, and treated populations. These dynamics suggest that individuals' behavior may change based on past disease outbreaks, highlighting the role of memory in disease transmission.

Based on the findings of this study, we recommend that the public continues to adhere to preventive measures, including reducing transmission rates, increasing vaccination uptake, and seeking timely medical treatment. Furthermore, governments should strengthen public health campaigns, improve healthcare infrastructure, ensure greater vaccine availability and accessibility, and continuously monitor and adapt policies to support ongoing research and development. By implementing these strategies, it is possible to reduce the spread of COVID-19 and protect the population from future outbreaks.

Author Contributions. **Akanni, J. O.**: Conceptualization, methodology, formal analysis, writing—original draft preparation, writing—review and editing, visualization. **Abidemi, A.**: Methodology, formal analysis, writing—review and editing, visualization, supervision. **Fatmawati, F.**: Methodology, validation, formal analysis, writing—review and editing. **Chukwu, C. W.**: Writing—review and editing, supervision.

Acknowledgement. The authors are thankful to the editors and reviewers who have supported us in improving this manuscript. We also placed on record to appreciate the input of Dr Joahua Kiddy Kwasi Asamoah who helped us to initially proofread this manuscript.

Funding. This research received no external funding.

Conflict of interest. The authors declare no conflict of interest.

Data availability. Not applicable.

References

[1] NHS. England, "Landmark moment as first nhs patient receives covid-19 vaccination,"2020, https://www.england.nhs.uk/2020/12/landmark-moment-as-first-nhs-patient-receives-covid-19-vaccination/, Accesed on 30 January 2025.

[2] E. Mathieu *et al.*, "Coronavirus pandemic (covid-19). our world in data," 2024, https://ourworldindata.org/coronavirus, Accesed on 30 January 2025.

[3] N. Imai *et al.*, "Interpreting estimates of coronavirus disease 2019 (covid-19) vaccine efficacy and effectiveness to inform simulation studies of vaccine impact: a systematic review," *Wellcome Open Res.*, vol. 6, p. 185, 2021. DOI:10.12688/wellcomeopenres.16992.1

[4] O. J. Wouters *et al.*, "Challenges in ensuring global access to covid-19 vaccines: production, affordability, allocation, and deployment," *The Lancet*, vol. 397, no. 10278, pp. 1023–1034, 2021. DOI:10.1016/S0140-6736(21)00306-8

[5] H. Wang *et al.*, "Estimating excess mortality due to the covid-19 pandemic: a systematic analysis of covid-19-related mortality, 2020–21," *The Lancet*, vol. 399, no. 10334, pp. 1513–1536, 2022. DOI:10.1016/S0140-6736(21)02796-3

[6] A. B. Hogan *et al.*, "Within-country age-based prioritisation, global allocation, and public health impact of a vaccine against sars-cov-2: a mathematical modelling analysis," *Vaccine*, vol. 39, no. 22, pp. 2995–3006, 2021. DOI:10.1016/j.vaccine.2021.04.002

[7] W. H. Organization, "Fair allocation mechanism for covid-19 vaccines through the covax facility," 2020, https://www.who.int/publications/m/item/fair-allocation-mechanism-for-covid-19-vaccines-through-the-covax-facility, Accesed on 30 January 2025.

[8] E. S. K. Besson *et al.*, "Excess mortality during the covid-19 pandemic: a geospatial and statistical analysis in aden governorate, yemen," *BMJ Glob Health*, vol. 6, no. 3, p. e004564, 2021. DOI:10.1136/bmjgh-2020-004564

[9] W. H. Organization, "Achieving 70% covid-19 immunization coverage by mid-2022," 2021, https://www.who.int/news/item/23-12-2021-achieving-70-covid-19-immunization-coverage-by-mid-2022, Accesed on 30 January 2025.

[10] S. Machingaidze and C. S. Wiysonge , "Understanding covid-19 vaccine hesitancy," *Nat. Med.*, vol. 27, no. 8, pp. 1338–1339, 2021. DOI:10.1038/s41591-021-01459-7

[11] D. Bernoulli, "Essai d'une nouvelle analyse de la mortalité causée par la petite vérole. mém," *Math Phys Acad Roy Sci Paris*, vol. 1, pp. 1–45, 1766.

[12] W. O. Kermack and A. G. McKendrick, "A contribution to the mathematical theory of epidemics," *Proc. R. Soc. Lond.*, vol. 115, no. 772, pp. 700–721, 1927

[13] F. Kemp *et al.*, "Modelling covid-19 dynamics and potential for herd immunity by vaccination in austria, luxembourg and sweden," *J. Theor. Biol.*, vol. 530, p. 110874, 2021. DOI:10.1016/j.jtbi.2021.110874

[14] C. Treesatayapun, "Model dynamics and optimal control for intervention policy of covid-19 epidemic with quarantine and immigrating disturbances," *Bull Math Biol.*, vol. 84, no. 11, p. 122, 2022. DOI10.1007/s11538-022-01080-w

[15] M. Rafiq *et al.*, "Numerical analysis of a bi-modal covid-19 sitr model," *Alex Eng J.*, vol. 61, no. 1, pp. 227–235, 2022. DOI:10.1016/j.aej.2021.04.102

[16] E. Acheampong *et al.*, "Mathematical modelling of earlier stages of covid-19 transmission dynamics in ghana," *Results Phys.*, vol. 34, p. 105193, 2022. DOI:10.1016/j.rinp.2022.105193

[17] Y. Liu, J. W. Tang, and T. T. Y. Lam, "Transmission dynamics of the covid-19 epidemic in england," *Int. J. Infect Dis.*, vol. 104, pp. 132–138, 2021. Doi:10.1016/j.ijid.2020.12.055

[18] S. M. Kassa, J. B. H. Njagarah, and Y. A. Terefe, "Analysis of the mitigation strategies for covid-19: from mathematical modelling perspective." *Chaos Solitons Fractals*, vol. 138, p. 109968, 2020. DOI: 10.1016/j.chaos.2020.109968

[19] K. S. Sharov , "Creating and applying sir modified compartmental model for calculation of covid-19 lockdown efficiency," *Chaos Solitons Fractals*, vol. 141, p. 110295, 2020. DOI:10.1016/j.chaos.2020.110295

[20] Z. W. Tong *et al.*, "Global transmission dynamic of sir model in the time of sars-cov-2," *Results Phys.*, vol. 25, p. 104253, 2021. DOI:10.1016/j.rinp.2021.104253

[21] Pai C, Bhaskar A, Rawoot V, "Investigating the dynamics of covid-19 pandemic in india under lockdown," *Chaos Solitons Fractals*, vol. 138, p. 109988, 2020. DOI:10.1016/j.chaos.2020.109988

[22] B. Huang *et al.*, "Integrated vaccination and physical distancing interventions to prevent future covid-19 waves in chinese cities," *Nat Hum Behav.*, vol. 5, no. 6, pp. 695–705, 2021. DOI:10.1038/s41562-021-01063-2

[23] P. Sah *et al.*, "Accelerated vaccine rollout is imperative to mitigate highly transmissible covid-19 variants," *EClinicalMedicine*, vol. 35, p. 100865, 2021. DOI:10.1016/j.eclinm.2021.100865

[24] M. A. Kuddus, M. Mohiuddin, and A. Rahman, "Mathematical analysis of a measles transmission dynamics model in bangladesh with double dose vaccination," *Sci. Rep.*, vol. 11, no. 1, p. 16571, 2021. DOI:10.1038/s41598-021-95913-8

[25] M. De la Sen *et al.*, "On a discrete seir epidemic model with two-doses delayed feedback vaccination control on the susceptible," *Vaccines*, vol. 9, no. 4, p. 398, 2021. DOI:10.3390/vaccines9040398

[26] M. G. Gomes *et al.*, "Individual variation in susceptibility or exposure to sars-cov-2 lowers the herd immunity threshold," *J. Theor. Biol.*, vol. 540, p. 111063, 2022. DOI:10.1016/j.jtbi.2022.111063

[27] S. Moore *et al.*, "Vaccination and non-pharmaceutical interventions for covid-19: a mathematical modelling study," *Lancet Infect. Dis.*, vol. 21, no. 6, pp. 793–802, 2021. DOI:10.1016/S1473-3099(21)00143-2

[28] P. Yang *et al.*, "The effect of multiple interventions to balance healthcare demand for controlling covid-19 outbreaks: a modelling study," *Sci Rep.*, vol. 11, no. 1, p. 3110, 2021. DOI:10.1038/s41598-021-82170-y

[29] D. Martínez-Rodríguez, G. Gonzalez-Parra, and R. Villanueva, "Analysis of key factors of a sars-cov-2 vaccination program: A mathematical modeling approach," *Epidemiologia.*, vol. 2, no. 2, pp. 140–161, 2021. DOI:10.3390/epidemiologia2020012

[30] A. Fuady *et al.*, "Targeted vaccine allocation could increase the covid-19 vaccine benefits amidst its lack of availability: A mathematical modeling study in indonesia," *Vaccines*, vol. 9, no. 5, p. 462, 2021. DOI:10.3390/vaccines9050462

[31] A. M. Ramos *et al.*, "Modeling the impact of sars-cov-2 variants and vaccines on the spread of covid-19," *Commun Nonlinear Sci Numer Simul.*, vol. 102, p. 105937, 2021. DOI:DOI:10.1016/j.cnsns.2021.105937

[32] E. F. Arruda *et al.*, "Modelling and optimal control of multi strain epidemics, with application to covid-19," *PLoS ONE*, vol. 16, no. 9, p. e0257512, 2021. DOI:10.1371/journal.pone.0257512

[33] U. A. de León, E. Avila-Vales, and K. Huang, "Modeling covid-19 dynamic using a two-strain model with vaccination," *Chaos Solitons Fractals*, vol. 157, p. 111927, 2022. DOI:10.1016/j.chaos.2022.111927

[34] A. Abidemi, Z. M. Zainuddin, and N. A. B. Aziz, "Impact of control interventions on COVID-19 population dynamics in Malaysia: a mathematical study," *The European Physical Journal Plus*, vol. 136, no. 2, p. 237, 2021. DOI:10.1140/epjp/s13360-021-01205-5

[35] F. Nyabadza *et al.*, "Modelling the potential impact of social distancing on the covid-19 epidemic in south africa," *Computational and mathematical methods in medicine*, vol. 2020, no. 1, p. 5379278, 2020. DOI:10.1155/2020/5379278

[36] M. A. Rois, Fatmawati, and C. Alfiniyah, "Two isolation treatments on the covid-19 model and optimal control with public education," *Jambura Journal of Biomathematics (JJBM)*, vol. 4, no. 1, pp. 88–94, 2023. DOI:10.34312/jjbm.v4i1.19963

[37] J. O. Akanni, Fatmawati, and C. W. Chukwu, "On the fractional-order modeling of covid-19 dynamics in a population with limited resources," *Communi. in Math. Bio. and Neurosci.*, vol. 2023, pp. 1–36, 2023. DOI:10.28919/cmbn/7875

[38] S. Olaniyi *et al.*, "Mathematical modelling and optimal cost-effective control of covid-19 transmission dynamics," *Eur. Phys. J.*, vol. 135(11):, pp. 1–20, 2020. DOI:10.1140/epjp/s13360-020-00954-z

[39] C. J. Edholm *et al.*, "A vaccination model for covid-19 in gauteng, south africa," *Infectious Disease Modelling*, vol. 7, no. 3, pp. 333–345, 2022. DOI:10.1016/j.idm.2022.06.002

[40] R. Syafitri, Trisilowati, and W. M. Kusumawinahyu, "Dynamics of covid-19 model with public awareness, quarantine, and isolation," *Jambura Journal of Biomathematics (JJBM)*, vol. 4, no. 1, pp. 63–68, 2023. DOI:10.34312/jjbm.v4i1.19832

[41] M. S. Islam *et al.*, "Covid-19 epidemic compartments model and bangladesh," *Preprints*, 2020. DOI:10.20944/preprints202004.0193.v1

[42] R. M. Yaseen *et al.*, "The modeling and mathematical analysis of the fractional-order of cholera disease: Dynamical and simulation," *Partial Differential Equations in Applied Mathematics*, vol. 12, p. 100978, 2024. DOI:10.1016/j.padiff.2024.100978

[43] R. M. Yaseen *et al.*, "Improving the hepatitis viral transmission model's dynamics by vaccination and contrasting it with the fractional-order model," *Partial Differential Equations in Applied Mathematics*, vol. 10, p. 100705, 2024. DOI:10.1016/j.padiff.2024.100705

[44] A. A. Mohsen, H. F. AL-Husseiny, and R. K. Naji, "The dynamics of coronavirus pandemic disease model in the existence of a curfew strategy," *Jour-*

nal of Interdisciplinary Mathematics, vol. 25, no. 6, pp. 1777–1797, 2022. DOI:10.1080/09720502.2021.2001139

[45] A. Ali and R. K. Naji, "Dynamical analysis within-host and between-host for hiv/aids with the application of optimal control strategy," *Iraqi Journal of Science*, vol. 61, no. 5, pp. 1173–1189, 2020. DOI:10.24996/ijs.2020.61.5.25

[46] A. M. Niger and A. B. Gumel, "Mathematical analysis of the role of repeated exposure on malaria transmission dyanmivs," *Differ. Equ. Dyn. Syst.*, vol. 16, no. 3, pp. 251–287, 2008. DOI:10.1007/s12591-008-0015-1

[47] S. Olaniyi, "Dynamics of zika virus model with nonlinear incidence and optimal control strategies," *Appl. Math. Inf. Sci.*, vol. 12, no. 5, pp. 969–982, 2018. DOI:10.18576/amis/120510

[48] J. O. Akanni, "Asymptotic stability of illicit drug dynamics with banditry compartment," *Appl. Math. Inf. Sci.*, vol. 14, no. 5, pp. 791–800, 2020. DOI:10.18576/amis/140506

[49] H. W. Hethcote, "The mathematics of infectious disease," *SIAM Review*, vol. 42, no. 4, pp. 599–653, 2000. DOI:10.1137/S0036144500371907

[50] P. Van den Driessche and J. Watmough, "Reproduction numbers and subthreshold endemic equilibria for compartmental models of disease transmission," *Mathematical Biosciences*, vol. 180, no. 1–2, pp. 29–48, 2002. DOI:10.1016/S0025-5564(02)00108-6

[51] A. Abidemi and N. A. B. Aziz , "Analysis of deterministic models for dengue disease transmission dynamics with vaccination perspective in Johor, Malaysia," *International Journal of Applied and Computational Mathematics*, vol. 8, no. 1, p. 45, 2022. DOI:10.1007/s40819-022-01250-3

[52] A. Abidemi, J. O. Akanni, and O. D. Makinde, "A non-linear mathematical model for analysing the impact of COVID-19 disease on higher education in developing countries," *Healthcare Analytics*, vol. 3, p. 100193, 2023. DOI:10.1016/j.health.2023.100193

[53] O. W. in Data, "Data on COVID-19 (coronavirus)," 2024, https://github.com/owid/covid-19-data/tree/master/public/data, Accessed 30 January 2025.

[54] J. O. Akanni, "A non-linear optimal control model for illicit drug use and terrorism dynamics in developing countries with time-dependent control variables," *Decision Analytics Journal*, vol. 8, p. 100281, 2023. DOI:10.1016/j.dajour.2023.100281

[55] D. Okuonghae and A. Omame, "Analysis of a mathematical model for COVID-19 population dynamics in Lagos, Nigeria," *Chaos, Solitons and Fractals*, vol. 139, p. 110032, 2020. DOI:10.1016/j.chaos.2020.110032

[56] I. Podlubny, "*Fractional differential equations*." San Diego: Academic Press, 1998.

[57] Z. M. Odibat and N. T. Shawagfeh, "Generalized taylor's formula," *Applied Mathematics Computation*, vol. 186, no. 1, pp. 286–293, 2007. DOI:10.1016/j.amc.2006.07.102

[58] S. Mangal, O. Misra, and J. Dhar, "Fractional-order deterministic epidemic model for the spread and control of hiv/aids with special reference to mexico and india," *Mathematics Computation Simulation*, vol. 210, pp. 82–102, 2023. DOI:10.1016/j.matcom.2023.03.008

[59] J. K. K. Asamoah *et al.*, "Global stability and cost-effectiveness analysis of covid-19 considering the impact of the environment: using data from Ghana," *Chaos, Solitons & Fractals*, vol. 140, p. 110103, 2020. DOI:10.1016/j.chaos.2020.110103

[60] S. Olaniyi and O. S. Obabiyi, "Qualitative analysis of malaria dynamics with nonlinear incidence function," *Applied Mathematical Sciences*, vol. 8, no. 78, pp. 3889–3904, 2014. DOI:10.12988/ams.2014.45326